



# Petrogenesis of microgranular enclaves in the A-type granitoid Krasnopol intrusion (Mazury Complex, northeastern Poland): Evidence of magma mixing

Justyna Domańska-Siuda<sup>1</sup> · Anna Grabarczyk-Gurba<sup>1</sup> · Krzysztof Nejbert<sup>1</sup>

Received: 11 December 2023 / Accepted: 29 June 2024 / Published online: 19 August 2024  
© The Author(s) 2024

## Abstract

The origin of magmatic microgranular enclaves has been investigated in the Mesoproterozoic granitoid Krasnopol intrusion (1.5 Ga), part of the AMCG (anorthosite–mangerite–charnockite–granite) Mazury Complex in the East European Craton (NE Poland). The granitoids are ferroan and metaluminous, and display the typical characteristics of A-type granites, with high contents of Zr, Nb, Ga and rare earth elements (REEs). The enclaves are metaluminous and have a broad compositional range with two groups distinguished: silica-poor (45–50 wt% SiO<sub>2</sub>) and silica-rich (54 to 59 wt% SiO<sub>2</sub>), the latter overlapping in composition with the granitoid samples. The silica-poor enclaves are enriched in REEs compared to the silica-rich type, while the silica-rich enclaves exhibit trace-element patterns similar to those of the granitoids. Initial whole rock  $\epsilon_{\text{Nd}}$  values range between -3.8 and -4.0 for the granitoids and give a slightly wider range from -2.6 to -3.8 for the enclaves. The  $^{87}\text{Sr}/^{86}\text{Sr}$  initial values vary from 0.7084 to 0.7138 for the granitoids and between 0.7052 and 0.7075 for the enclaves and indicate that the granitoids and enclaves are not isotopically identical. These may suggest that the two magmatic systems represented by the granitoid host rock and the enclaves, were probably derived from different sources, but with sufficient interaction, which led to a progressive change in the composition of the enclaves towards intermediate composition. We suggest that the mafic melts of the enclaves were generated at the base of the thickened crust through partial melting of the lower crustal source, with a significant contribution from mantle material. The increase in temperature resulted in anatexis of the lower crust and the formation of the granitoid parental magma.

**Keywords** A-type granitoids · Magmatic microgranular enclaves · Magma mixing-mingling · AMCG magmatism · Mazury Complex · East European Craton

## Introduction

A-type granitoids have been described in many Proterozoic crystalline domains, where they are closely associated in space and time with anorthosites, mangerites and charnockites, together constituting AMCG suites, which play a crucial role in the formation of the Proterozoic crust. Well-documented examples of A-type or rapakivi granitoids, occurring within the crystalline basement of the East European Craton (EEC), come from Ukraine (Shumlyansky et al.

2017) Finland (Rämö and Haapala 1995), Estonia (Rämö et al. 1996), Latvia (Rämö et al. 1996) Lithuania (Skridlaite et al. 2003; Vejelyte et al. 2015), south Sweden (Čečys et al. 2002; Čečys and Benn 2007), the Danish island of Bornholm (Zariņš and Johansson 2009; Waight et al. 2012; Johansson et al. 2016) and Poland (Bagiński et al. 2001, 2007; Duchesne et al. 2010). All massifs show features typical of anorogenic/post-collisional affinity, with elevated contents of incompatible elements and REEs (Haapala and Rämö 1999). The crystallization age of the anorogenic rapakivi intrusions, recognized in the crystalline basement of the EEC, is in the wide range of 1.81–1.47 Ga (Rämö and Haapala 1995; Haapala and Rämö 1999; Zariņš and Johansson 2009; Shumlyansky et al. 2017).

Microgranular, magmatic enclaves are common within calc-alkaline and alkaline granitoids (Didier 1973, 1984; Barbarin and Didier 1991; Eklund et al. 1994; Salonsaari

Editorial handling: X. Xu

✉ Justyna Domańska-Siuda  
j.domanska@uw.edu.pl

<sup>1</sup> Faculty of Geology, University of Warsaw, Żwirki i Wigury 93, 02-089 Warsaw, Poland

and Haapala 1994; Skridlaite et al. 2003; Guimarães et al. 2005; Bogaerts et al. 2006; Yang et al. 2006; Bonin 2007; Słaby and Martin 2008; Teng et al. 2009; Shellnutt, et al. 2010; Domańska-Siuda et al. 2019; Kontonikas-Charos et al. 2023; Narshima and Kumar 2023) being invaluable material for research on mafic-felsic magma interactions. The study of enclaves, their textures, compositions and relationships with the host rocks, may provide important information on the origin and evolution of the magmatic system in which they were emplaced (e.g., Didier 1973; White and Chappell 1977; Vernon 1984; Barbarin and Didier 1991; Barbarin 2005; Kumar and Rino 2006; Bonin 2007).

Different models have been proposed for the origin of enclaves. The ‘restite model’, proposed by Chappell et al. 1987, Chappell and White (1991 and references therein), interpreted the enclaves as representative of the solid residues of refractory minerals from the partial melting of the granitoid source rocks. Such enclaves should have metamorphic or residual sedimentary textures inherited from the source. Dorais et al. (1997), Fershtater and Borodina (1977, 1991), Donaire et al. (2005), Shellnutt et al. (2010) and Flood and Shaw (2014), proposed the ‘autolith model’ (named also ‘cognate’ or ‘cumulate’ model), in which enclaves have a cognate origin with their host and represent disrupted cumulates or the fine-grained (early precipitating) chilled margin of the magma chamber. Therefore, the microgranular texture of enclaves can be explained by the rapid cooling of magma, e.g., at marginal parts of the magma chamber or roof zones and margins of magma conduits (Donaire et al. 2005). Temperatures below the liquidus, quenching and rapid crystallization of more mafic minerals are thus inevitable because of the thermal contrast in such cases. Such chilled material should be split, incorporated into the magma chamber and dispersed by convection to form enclaves. Alternatively, the enclaves may be treated as mafic magma ‘globules’ or ‘blobs’ (Didier 1973; Vernon 1984, 1991; Castro et al. 1990; Barbarin and Didier 1991; Reid et al. 1993; Elburg 1996; Collins et al. 2000; Kumar and Rino 2006; Słaby and Martin 2008; Perugini and Poli 2012; Chen et al. 2015; Kumar 2020, and others), which have mingled or partly mixed with felsic magmas (‘magma mixing’ model). Mingling permits only limited chemical and mineral exchange between the mafic and felsic magmas shifting the chemical composition of the enclaves towards felsic host values. Mafic blobs are dispersed through the pluton by convection (Didier and Barbarin 1991) or by ascent and decompression of the enclave-rich zone due to gravitational instability and fluidization (Wang et al. 2011). The last two models assume that the enclaves are of magmatic origin.

In this study, we focus on the A-type Krasnopol granitoid intrusion, part of the AMCG Mazury Complex in the EEC (NE Poland; Fig. 1A, B), where microgranular enclaves are common. To specify the genetic model we carried out

whole-rock chemical analyses, Sr–Nd isotope ratio measurements and electron microprobe analyses of the enclaves and their host rocks on selected drill core fragments of the Krasnopol intrusion.

## Geological setting

The Fennoscandian, Sarmatian and Volgo-Uralian crustal segments (Fig. 1A) constitute the EEC, which forms the crystalline basement of northeastern Europe. Fennoscandia was formed during the long-lasting subduction-collision episodes of the Svecofennian orogeny at ca. 1.9–1.8 Ga (e.g., Bogdanova et al. 2015; Salminen et al. 2021; Skridlaite et al. 2021). The crystalline basement of northeastern Poland represents part of the Fennoscandian craton, located south of its exposed part in the Fennoscandian (Baltic) Shield, (Fig. 1A) and buried beneath Cambrian to Cenozoic sedimentary strata. The major Paleoproterozoic tectonic units in the basement of northeastern Poland are the Mazowsze (MD), Dobrzyń (DD) and Pomorze-Blekinge Belt (PB) domains (Fig. 1B; Krzemińska et al. 2017), which extend to the SW margin of the EEC defined by the Teisseyre-Tornquist Zone (TTZ; Fig. 1B; Dadlez et al. 2005).

During the Mesoproterozoic, at ca. 1520–1500 Ma, northeastern Poland was affected by intense bimodal and multi-stage magmatism consisting of several small bodies forming the Mazury Complex (MC; Fig. 1B). The MC is dominated by granitoids of leucogranite to granodiorite and monzodiorite composition (Bagiński et al. 2001; Wiszniewska et al. 2002, 2007; Duchesne et al. 2010). The significant components are mafic-intermediate (anorthositic-gabbroitic-noritic) bodies of the Kętrzyn, Suwałki and Sejny massifs (Wiszniewska et al. 2002; Grabarczyk and Wiszniewska 2019) enveloped by charnockites and diorites (Petecki and Wiszniewska 2021). Therefore, the MC, which extends from the Baltic Sea shore, through the northern border of Poland, to the Kabeliai and Veisiejai complexes in Lithuania (Skridlaite et al. 2003, 2008), is an example of the widespread in Proterozoic, AMCG (anorthosite-mangerite-charnockite-granitoid) magmatism. The MC extends latitudinally over 300 km and can be linked to deep, E–W trending, crustal discontinuities or shear zones.

The Krasnopol granitoid intrusion, located in the eastern part of the MC, is concealed under 586 m of sedimentary strata and drilled by the Krasnopol PIG-6 borehole (Kr-6; Fig. 1B), which reveals monzodiorite and granodiorite as the main constituents (Dörr et al. 2002). The composition of the Krasnopol granitoids is similar to those from the Pawłówka PIG-1 (Pw), Filipów IG1 (Fp) and Bartoszyce IG1 (Br) boreholes (Fig. 1B; Bagiński et al. 2001). With SiO<sub>2</sub> contents of 55.6–62.1 wt%, metaluminous character and an elevated content of REEs (371–557 ppm) the Krasnopol rocks show geochemical

characteristics of A-type granitoids (Bagiński et al. 2001; Dörr et al. 2002). The Krasnopol ‘rapakivi-like’ granitoids yielded zircon thermal-ionization mass spectrometry (TIMS) U–Pb age of  $1516 \pm 1.1$  Ma (Dörr et al. 2002), whereas granitoids lacking rapakivi porphyritic texture were recently dated to  $1507 \pm 6$  Ma using the sensitive high-resolution ion microprobe (SHRIMP) U–Pb zircon analyses (Wiszniewska and Krzemińska 2021). Abundant microgranular enclaves of mafic and intermediate composition, recorded only in the Krasnopol body, are spatially associated with granitoids.

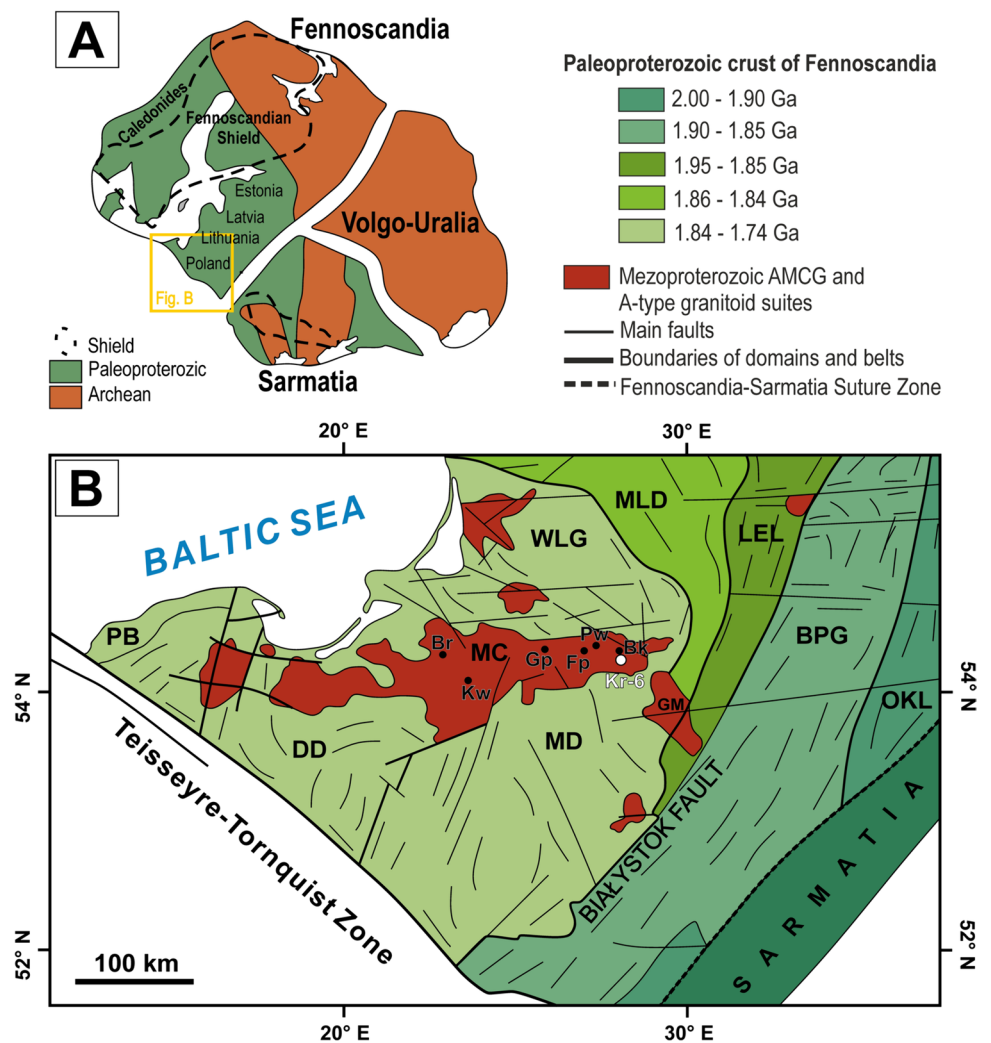
## Analytical methods

### Whole-rock geochemistry

Based on thin-section analyses, twenty-one samples from the Krasnopol PIG-6 drill core ( $23^\circ 13' 52''\text{E}$ ,  $54^\circ 07' 13''\text{N}$ ; 10 km west of Sejny village) from different depths

were selected for geochemical studies, i.e., seven granitoid samples, of which four (marked with G index) were taken at a cm distance from the granite/enclave contact; eight samples of the enclaves that made up the entire drill core; and six samples of the enclaves were taken at a cm distance from the granitoid/enclave contact. The samples with the granitoid/enclave contact were cut using a saw, and central parts were taken for geochemical analyses to preserve their representative composition. Each sample was crushed and quartered, and 100 g of each rock was milled into powder. Major elements contents were measured by means of a Spectro Ciros Vision inductively coupled plasma-emission spectrometer (ICP-ES), and trace elements concentrations were measured by PerkinElmer ELAN 6000 or ELAN 9000 inductively coupled plasma-mass spectrometers (ICP-MS). Detection limits for each element are listed in Table 1. All analyses were recalculated on an anhydrous basis, with iron expressed as total  $\text{Fe}_2\text{O}_3$  ( $\text{Fe}_{2\text{O}_{3\text{t}}} = \text{Fe}_2\text{O}_3 + 1.111 \text{ FeO}$ ).

**Fig. 1** A Sketch showing the distribution of the main shield areas in relation to the three Precambrian crustal blocks in the East European Craton (Gorbatshev and Bogdanova 1993; modified) and B sketch map of the major crustal domains within the part of the East European Craton (Bogdanova et al. 2015; modified). Crustal domains: BPG – Belarus-Podlasie Granulite Belt, DD – Dobrzyń Domain, GM – Grodno Massif, LEL – Latvian-East Lithuanian Belt, MC – Mazury Complex, MD – Mazowsze Domain, MLD – Mid-Lithuanian Domain, PB – Pomorze-Blekinge domain, WLG – West Lithuanian Granulite Domain. Boreholes (black dots): Bk – Boksze IG1, Br – Bartoszyce IG1, Fp – Filipów IG1, Gp – Gołdap IG1, Kr-6 – Krasnopol PIG-6, Kw – Klewno IG1, Pw – Pawłówka PIG-1



## Mineral chemistry

Compositions of minerals in selected thin sections were determined using the CAMECA SX-100 electron probe microanalyser (EPMA) equipped with wavelength-dispersive spectrometers (WDS). Prior to analysis, samples were coated with C for conductivity. The following conditions were applied: acceleration voltage 15 kV; beam current 10 nA (biotite, feldspars), 20 nA (amphibole, pyroxene) and 30 nA (zircon), respectively; focal-spot diameter from 1 to 5  $\mu\text{m}$  depending on the analysed mineral; 20 s and 10 s counting times for peak and background positions, respectively. The spectral interferences of the rare earth element (REE) analytical lines were automatically corrected in the quantitative result files by the SX-100 software. During the quantification procedure, the interference intensity of the overlapping lines calculated from the measurement on the standard was taken into account. The matrix correction was performed using the standard ZAF procedure (Merlet 1994). Reference materials and standards, selected analytical lines, diffracting crystals, peak and background counting times were as follow: Na (albite,  $K\alpha$ , TAP, 15 s, 20 s); Mg (diopside,  $K\alpha$ , TAP, 20 s, 10 s for feldspars and 30 s, 20 s for titanite); Si (diopside,  $K\alpha$ , TAP, 20 s, 10 s); Ca (diopside,  $K\alpha$ , PET, 20 s, 10 s for feldspars and 30 s, 25 s for titanite); K (orthoclase,  $K\alpha$ , PET, 20 s, 10 s); Al (orthoclase,  $K\alpha$ , TAP, 20 s, 10 s for feldspars and 30 s, 20 s for titanite); Fe (hematite,  $K\alpha$ , LIF, 40 s, 20 s); Mn (rhodonite,  $K\alpha$ , LIF, 40 s, 20 s); P ( $\text{YPO}_4$ ,  $K\alpha$ , PET, 30 s, 20 s); Ba (barite,  $L\alpha$ , LPET, 30 s, 15 s for feldspar and 60 s, 30 s for mica); Ti (rutile,  $K\alpha$ , PET, 40 s, 20 s); Zr (zircon,  $L\alpha$ , LPET, 30 s, 15 s); F (phlogopite,  $K\alpha$ , TAP, 15 s, 15 s); Cr (synthetic  $\text{Cr}_2\text{O}_3$ ,  $K\alpha$ , LPET, 30 s, 15 s); Ni (synthetic NiO,  $K\alpha$ , LIF, 30 s, 20 s); Cl (tugtupite,  $K\alpha$ , LPET, 20 s, 10 s).

## Sr–Nd isotopes

Samples for Nd isotopic analyses were ground to a fine powder with an agate mortar and pestle. The chemical separations of Nd, Sm and Sr, as well as measurements of their isotopic composition, were carried out in the Isotope Laboratory at the University of Poznań. For Sm and Nd concentration determination about 50 mg of powdered rock sample was spiked with a  $^{150}\text{Nd}$ – $^{149}\text{Sm}$  tracer solution and dissolved on a hot plate (~100 °C, 3 d) in a mixture of concentrated ultrapure hydrofluoric and nitric acid (4:1). The miniaturized chromatographic techniques described by Pin et al. (1994) were applied for REE, Rb and Sr separation. Some modifications to the column size and concentration of reagents were introduced by Dopieralska (2003). Strontium was loaded with a  $\text{TaCl}_5$  activator on a single Re filament,

whereas Nd and Sm (loaded as phosphate) were measured in a Re double filament configuration on a Finnigan MAT 261 thermal ionization mass spectrometer. The Nd and Sr isotopic compositions were measured in multidynamic, and Sm in static mode.

Initial  $^{87}\text{Rb}/^{86}\text{Sr}$  ratios were calculated from measured  $^{87}\text{Sr}/^{86}\text{Sr}$  ratio and Rb and Sr analyses given in Table 1. The NBS 987 Sr standard gave  $^{87}\text{Sr}/^{86}\text{Sr}$  of  $0.710226 \pm 11$  ( $2\sigma$  mean on 22 analyses). Measurements of the AMES standard yielded  $^{143}\text{Nd}/^{144}\text{Nd} = 0.512129 \pm 10$  ( $2\sigma$  mean on 20 analyses). Total procedure blanks were less than 35 pg for Nd and Sm, and less than 80 pg for Sr. Nd isotope data are reported in the standard epsilon notation ( $\epsilon$ ) calculated using  $^{143}\text{Nd}/^{144}\text{Nd} = 0.512638$  and  $^{147}\text{Sm}/^{144}\text{Nd} = 0.1967$  for present-day (0) chondritic uniform reservoir ( $\text{CHUR}_0$ ) (Jacobsen and Wasserburg 1980). All  $\epsilon_{\text{Nd}}$  values are recalculated according to the measured  $^{147}\text{Sm}/^{144}\text{Nd}$  ratios for the time of intrusion (t). Depleted mantle model ages ( $T_{\text{DM}}$ ; DePaolo 1983) are calculated assuming present-day depleted mantle values of  $^{147}\text{Sm}/^{144}\text{Nd} = 0.2137$  and  $^{143}\text{Nd}/^{144}\text{Nd} = 0.513151$ .

## Results

### Petrography

The A-type Krasnopol granitoid intrusion consists of porphyritic monzonite and granodiorite and hosts numerous intermediate to mafic rocks, with monzonite, monzodiorite and monzogabbro composition, referred to as microgranular enclaves (Fig. 2A–H). Granitoids are typically greyish, medium to coarse-grained massive rocks, with large (up to 3 cm) K-feldspar and plagioclase phenocrysts (Figs. 2A, C, D and 3A, D). Locally, the granitoids exhibit a linear fabric, likely caused by magmatic flow. The groundmass is composed of plagioclase, K-feldspar, quartz and biotite, with amphibole, clinopyroxene and Fe-Ti oxides as minor constituents (Fig. 3A, D, F). Myrmekites are abundant. Accessory minerals are prismatic apatite, present as inclusions in mafic minerals, euhedral to rounded zircon (abundant in biotite) and titanite occurring typically as rims around magnetite and ilmenite. Monazite, allanite and chevkinite-group minerals are less common. In some samples, ilmenite-magnetite aggregates of irregular, lobate shapes (Fig. 3F) intergrown with subhedral plagioclase can be observed. Aggregates are mantled by two types of biotite, i.e., the inner rim is built of small laths of biotite, while the outer one consists of larger crystals. Opaque minerals are interstitial to feldspars, with complex oxyexsolution textural relationships.

**Table 1** Results of chemical analyses of the granitoid rocks and magmatic microgranular enclaves from the Krasnopol FIG 6 borehole

Sample	DL	KR-6-3	KR-6-18	KR-6-31	KR-6-50G	KR-6-57G	KR-6-59G	KR-6-62G	KR-6-37	KR-6-48	KR-6-57
Depth		661 m	1100.8 m	1469 m	992.6 m	1253 m	1281 m	1444.8 m	785 m	981 m	1253 m
Lithology		GR	GR	GR	GR	GR	GR	GR	SP-ME	SP-ME	SP-ME
Major oxides (wt %)											
SiO <sub>2</sub>	0.01	62.12	60.85	58.71	61.89	55.59	60.04	59.76	45.50	47.02	48.71
TiO <sub>2</sub>	0.01	1.17	1.49	1.65	1.33	1.95	1.51	1.54	3.29	3.22	2.80
Al <sub>2</sub> O <sub>3</sub>	0.01	15.40	14.86	15.12	14.99	15.28	15.07	15.09	15.29	14.14	15.16
Fe <sub>2</sub> O <sub>3t</sub>	0.04	6.82	8.16	9.82	7.24	11.75	8.38	9.07	16.25	16.13	14.42
Cr <sub>2</sub> O <sub>3</sub>	0.002	<0.002	<0.002	<0.002	<0.002	0.004	0.002	0.002	<0.002	<0.002	<0.002
MnO	0.01	0.11	0.12	0.14	0.12	0.16	0.13	0.12	0.32	0.33	0.27
MgO	0.01	1.64	1.98	2.11	1.77	2.31	1.89	1.77	3.63	3.21	3.70
CaO	0.01	3.51	4.40	4.88	4.42	5.15	4.39	3.90	8.66	7.31	7.38
Na <sub>2</sub> O	0.01	2.52	2.70	2.89	2.70	2.85	2.56	2.62	3.15	2.45	3.04
K <sub>2</sub> O	0.01	5.52	4.23	3.63	4.18	3.52	4.80	5.02	1.91	4.11	3.31
P <sub>2</sub> O <sub>5</sub>	0.01	0.31	0.40	0.44	0.41	0.67	0.47	0.44	0.91	1.15	0.73
LOI	-5.1	0.40	0.40	0.20	0.50	0.30	0.30	0.20	0.70	0.40	0.05
Total		99.52	99.59	99.59	99.55	99.53	99.54	99.53	99.61	99.47	99.52
A/CNK		0.93	0.87	0.86	0.88	0.86	0.87	0.90	0.66	0.65	0.69
Mg#		0.32	0.32	0.30	0.33	0.28	0.31	0.28	0.31	0.28	0.34
Trace elements (ppm)											
Ba	1	2502	1789	1507	1797	1252	1860	1773	659	1708	1416
Cs	1	1.5	0.8	1.0	0.9	1.1	0.9	1.6	0.9	0.9	1.0
Ga	0.5	23.4	22.7	23.2	16.8	22.4	19.6	20.4	23.7	23.5	23.2
Rb	0.1	129.5	168.4	114.0	116.0	118.2	128.3	149.7	73.9	85.4	109.8
Sr	0.5	377.6	405.0	383.1	363.8	336.0	351.6	334.6	373.5	352.4	383.4
V	8	87	104	131	104	175	116	132	168	206	227
Co	0.2	15.1	18.4	18.2	14.0	22.7	16.7	15.7	32.1	28.3	25.8
Ni	20	<20	<20	<20	<20	<20	<20	<20	<20	<20	<20
Zr	0.1	344.8	372.1	559.3	655.4	734.2	483.3	618	391.9	547.8	574.9
Hf	0.1	8.1	8.7	13.1	15.3	17.6	11.7	15.1	9.7	13.1	14.5
Y	0.1	31.8	36.9	38.4	46.7	58.4	40.3	40.5	83.1	98.4	85.7
Nb	0.1	15.5	19.6	21.6	18.4	26.4	20.1	18.7	49.1	52.7	38.2
Ta	0.1	0.9	0.8	1.2	0.9	1.2	1.0	1.0	2.4	2.6	1.3
U	0.1	0.8	0.6	0.8	0.4	1.5	0.9	1.5	0.4	1.1	0.5
Th	0.2	11.2	8.5	8.0	14.5	13.1	11.0	16.4	4.0	5.5	4.0
La	0.1	82.5	89.3	88.3	100.0	114.3	92.1	94.4	123.1	137	113.4
Ce	0.1	165.5	179.2	180.4	197.2	233.9	175.3	179.5	268.4	304.2	257.3
Pr	0.02	18.4	20.1	20.8	30.0	29.1	21.6	22.0	33.4	40.3	32.14
Nd	0.3	78.1	68.1	77.6	96.1	113.6	80.3	81.7	132.3	162.2	132.9
Sm	0.05	12.1	10.3	13.9	16.5	19.0	13.6	13.4	24.9	29.5	24.2

Table 1 (continued)

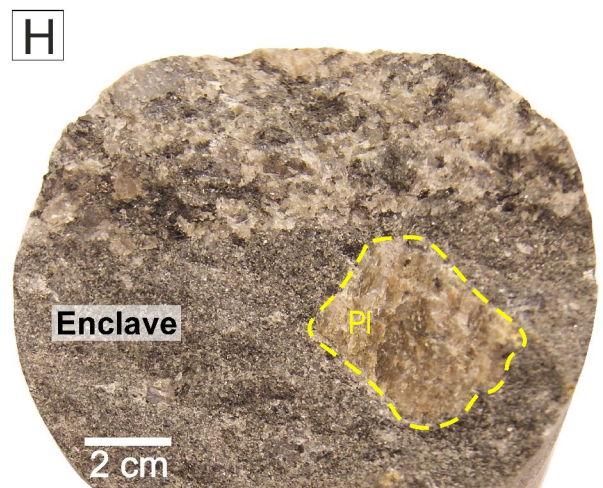
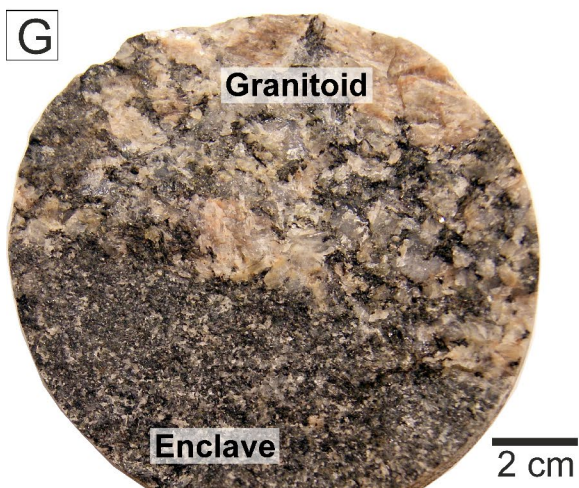
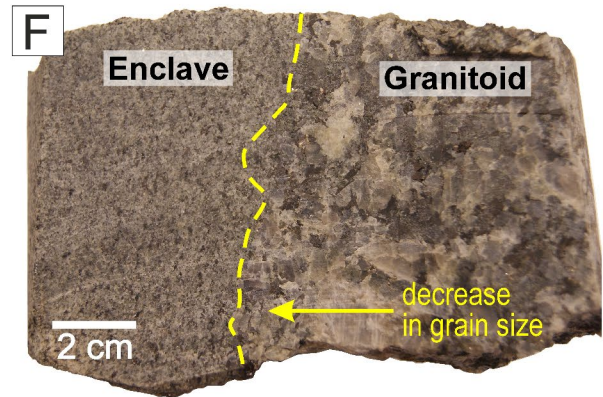
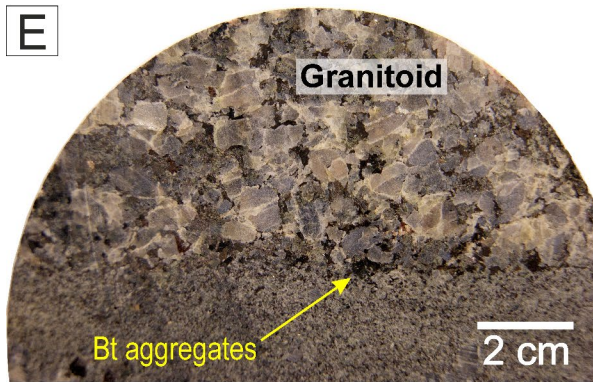
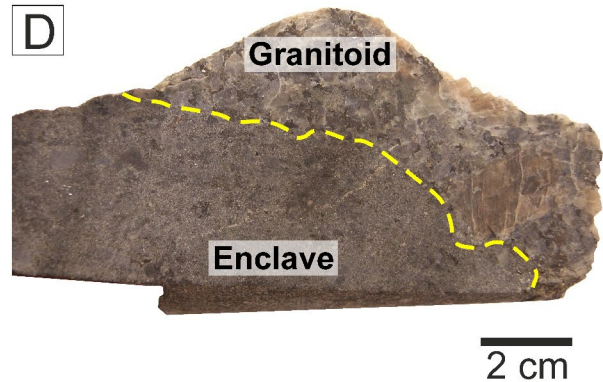
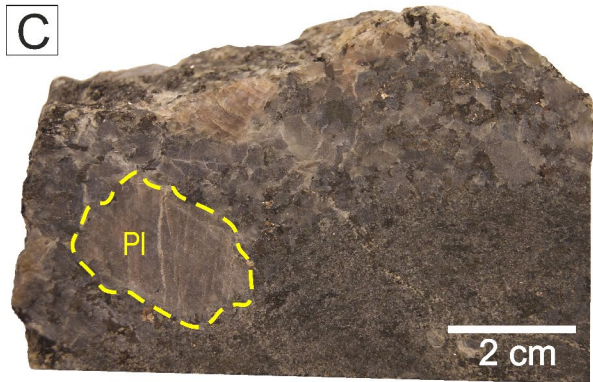
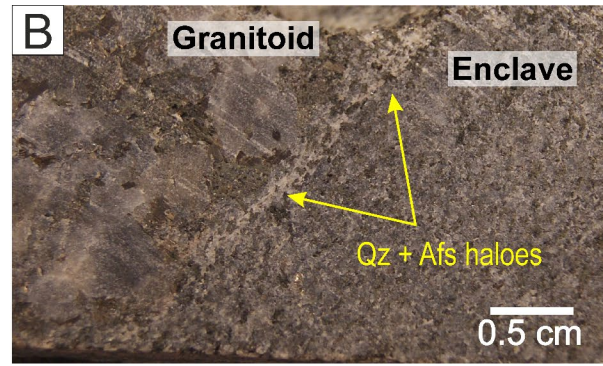
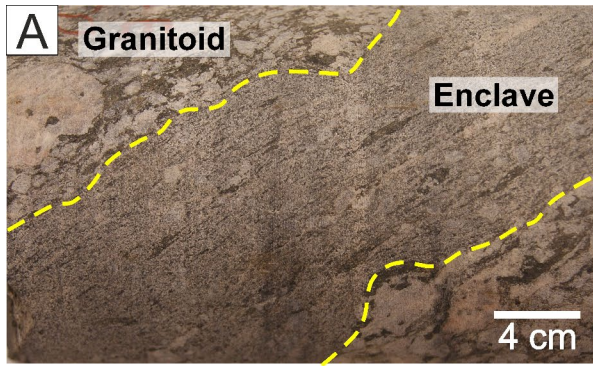
Sample	DL	KR-6-3	KR-6-18	KR-6-31	KR-6-50G	KR-6-57G	KR-6-59G	KR-6-62G	KR-6-37	KR-6-48	KR-6-57
Depth		661 m	1100.8 m	1469 m	992.6 m	1253 m	1281 m	1444.8 m	785 m	981 m	1253 m
Lithology		GR	GR	GR	GR	GR	GR	GR	SP-ME	SP-ME	SP-ME
Eu	0.02	3.1	3.2	3.3	3.3	3.7	3.2	3.2	3.9	4.6	4.1
Gd	0.5	8.2	12.0	10.7	13.7	15.6	11.0	10.9	21.6	25.9	21.9
Tb	0.01	1.2	1.3	1.5	1.9	2.2	1.5	1.5	3.1	3.6	2.9
Dy	0.05	5.9	7.6	8.4	10.3	11.6	8.1	8.0	16.8	19.7	17.0
Ho	0.02	1.2	1.4	1.6	2.0	2.2	1.5	1.5	3.0	3.8	3.1
Er	0.03	3.2	3.8	4.1	5.3	6.0	4.2	4.0	8.7	10.5	8.1
Tm	0.01	0.4	0.5	0.6	0.7	0.8	0.5	0.5	1.2	1.4	1.1
Yb	0.05	2.8	3.2	3.3	4.4	4.8	3.4	3.4	7.3	8.6	6.8
Lu	0.01	0.4	0.4	0.5	0.6	0.7	0.5	0.5	1.0	1.2	0.9
(La/Yb) <sub>N</sub>		19.7	18.8	17.6	15.1	15.9	18.2	18.3	11.3	10.6	11.2
Eu/Eu*		1.05	0.82	0.84	0.68	0.66	0.80	0.81	0.51	0.51	0.54
ΣREE		371.1	412.3	415.1	477.0	557.4	416.8	424.6	648.8	752.6	625.7
Sample	KR-6-45	KR-6-61	KR-6-35	KR-6-42	KR-6-53	KR-6-58	KR-6-47	KR-6-63	KR-6-59	KR-6-50	KR-6-54
Depth	924 m	1380 m	650 m	862 m	1103.8 m	1269 m	975.5 m	1449 m	1281 m	992.6 m	1154 m
Lithology	SP-ME	SP-ME	SR-ME	SR-ME	SR-ME	SR-ME	SR-ME	SR-ME	SR-ME	SR-ME	SR-ME
Major oxides (wt %)											
SiO <sub>2</sub>	49.06	50.25	53.33	54.13	56.11	56.32	56.51	57.46	57.67	58.74	58.76
TiO <sub>2</sub>	2.96	2.93	2.16	2.52	2.01	2.34	2.15	2.00	2.19	1.72	1.81
Al <sub>2</sub> O <sub>3</sub>	14.67	14.64	15.93	14.17	15.52	14.35	14.76	14.73	13.45	14.20	14.77
Fe <sub>2</sub> O <sub>3t</sub>	14.55	14.48	11.46	12.49	10.34	11.28	10.84	10.36	10.85	9.96	9.49
Cr <sub>2</sub> O <sub>3</sub>	<0.002	<0.002	0.002	<0.002	<0.002	<0.002	0.002	<0.002	0.002	0.003	<0.002
MnO	0.30	0.29	0.20	0.22	0.16	0.20	0.18	0.19	0.18	0.16	0.18
MgO	3.42	3.23	2.97	2.89	2.24	2.66	2.56	2.24	2.37	2.40	1.79
CaO	7.40	7.13	6.21	5.84	6.05	5.74	5.03	5.80	5.96	4.94	4.76
Na <sub>2</sub> O	2.85	3.06	3.25	2.61	2.96	2.63	2.67	2.88	2.52	2.47	2.89
K <sub>2</sub> O	2.86	2.40	2.58	3.44	3.06	3.08	4.00	3.21	3.51	3.68	4.10
P <sub>2</sub> O <sub>5</sub>	1.07	0.88	0.74	0.82	0.62	0.59	0.53	0.57	0.62	0.55	0.66
LOI	0.40	0.30	0.80	0.40	0.50	0.40	0.30	0.20	0.20	0.70	0.30
Total	99.54	99.59	99.63	99.53	99.57	99.59	99.53	99.64	99.52	99.52	99.51
A/CNK	0.69	0.71	0.82	0.76	0.81	0.79	0.83	0.79	0.72	0.83	0.83
Mg#	0.32	0.31	0.34	0.31	0.30	0.32	0.32	0.30	0.30	0.32	0.27
Trace elements (ppm)											
Ba	1269	1100	1093	1383	1281	1284	1760	1325	1589	1391	2067



Table 1 (continued)

Sample	KR-6-45	KR-6-61	KR-6-35	KR-6-42	KR-6-53	KR-6-58	KR-6-47	KR-6-63	KR-6-59	KR-6-50	KR-6-54
Depth	924 m	1380 m	650 m	862 m	1103.8 m	1269 m	975.5 m	1449 m	1281 m	992.6 m	1154 m
Lithology	SP-ME	SP-ME	SR-ME	SR-ME	SR-ME	SR-ME	SR-ME	SR-ME	SR-ME	SR-ME	SR-ME
Cs	0.3	0.4	0.3	0.5	0.4	0.3	0.5	0.2	0.4	1.1	0.4
Ga	22.5	21	22.1	22.8	21.8	20.7	21.4	18.3	21.8	21.6	20.6
Rb	71.7	62.6	74.4	92.5	86.3	82.3	101.7	81.8	94.2	123.9	94.9
Sr	394.2	379.4	384.9	341.4	374.3	340.8	365.0	379.7	336.7	306.5	396.3
V	175	179	160	150	137	170	168	136	194	132	76
Co	27.7	26.6	26.5	23.9	19.5	22.5	22.3	17.6	22.1	20.0	13.8
Ni	<20	<20	<20	<20	<20	<20	<20	<20	<20	<20	<20
Zr	549.7	408.7	394.8	558.6	620.7	456.3	376.9	344.6	579.5	638.8	682.3
Hf	13.3	9.7	8.7	13.2	14.5	11.1	8.8	8.2	13.9	15.3	15.1
Y	79.7	77.8	50.0	59.5	48.6	43.1	40.8	41.0	57.8	51.0	55.4
Nb	49.3	46	28.3	34.7	25.8	21.9	19.8	29.5	26.5	22.1	22.3
Ta	2.6	2.2	1.5	1.7	1.3	1.3	1.0	1.4	1.2	1.1	1.0
U	0.3	0.6	0.4	0.6	0.5	0.4	0.5	0.1	0.4	1.3	0.3
Th	4.0	5.2	4.5	3.4	2.8	3.0	4.2	1.4	4.8	5.6	2.1
La	115.8	126.3	102.1	92.5	81.5	80.1	75.9	75.0	122.7	142.2	89.1
Ce	257.7	271.6	219	191.0	166.8	156.7	146.4	151.8	241.4	282.6	197.1
Pr	32.3	32.7	25.3	24.7	21.5	20.31	18.4	18.3	29.8	31.3	23.5
Nd	130.4	129.9	100.0	97.3	85.9	76.8	70.9	75.0	112.9	113.1	95.6
Sm	23.9	22.7	17.2	17.5	14.5	13.7	12.2	13.4	18.3	17.6	17.9
Eu	4.1	3.6	3.4	3.7	3.4	3.1	3.4	3.1	3.6	3.3	4.5
Gd	21.4	19.5	13.8	15.3	12.6	11.4	10.7	11.1	14.7	13.1	15.4
Tb	2.8	2.6	1.8	2.2	1.7	1.6	1.5	1.6	2.1	1.65	2.1
Dy	16.3	14.4	10.3	11.6	9.5	8.3	8.1	9.0	11.5	9.5	12.2
Ho	2.9	2.8	1.8	2.2	1.8	1.7	1.5	1.6	2.3	1.6	2.1
Er	7.9	7.6	5.3	6.2	4.9	4.4	4.2	4.6	6.2	4.7	5.6
Tm	1.1	0.9	0.7	0.8	0.7	0.6	0.6	0.6	0.8	0.6	0.8
Yb	6.9	6.3	4.3	5.0	4.1	3.7	3.5	3.7	5.2	3.7	4.6
Lu	0.9	0.9	0.6	0.8	0.6	0.6	0.6	0.6	0.7	0.6	0.7
(La/Yb) <sub>N</sub>	11.2	13.3	15.8	12.3	13.4	14.4	14.5	13.5	15.9	25.6	13.0
Eu/Eu*	0.56	0.53	0.68	0.69	0.78	0.76	0.92	0.78	0.68	0.67	0.84
ΣREE	624.6	642.1	505.7	470.7	409.7	383.0	358.0	369.4	572.4	625.5	471.2

GR granitoid, SP-ME silica-poor enclave, SR-ME silica-rich enclave, DL detection limits, LOI loss on ignition, A/CNK Al<sub>2</sub>O<sub>3</sub>/(CaO+Na<sub>2</sub>O+K<sub>2</sub>O) molar, Mg# MgO/(MgO+FeO), Eu/Eu\* [Eu<sub>N</sub>√(Sm<sub>N</sub>×Gd<sub>N</sub>)], N chondrite (C1) normalized to values of Nakamura (1974)





**Fig. 2** Field photographs of studied rocks and their textures: **A** magmatic foliation in the enclave; **B** enclave surrounded by narrow felsic halo; **C** feldspar phenocrysts crossing the contacts between the enclave and granitoid; **D** diffuse contact between the enclave and granitoid; **E** sharp contact between the enclave and granitoid marked by the presence of mafic minerals; **F** sharp contact between the enclave and granitoid with visible decrease in the grain size closer to the border; **G** sharp contact between the fine-grained enclave and coarse-grained granitoid; **H** feldspar phenocrysts within the fine-grained enclave. Afs – alkali feldspar, Bt – biotite, Pl – plagioclase, Qz – quartz

Microgranular enclaves are spatially associated with granitoid rocks. The real size and form of the enclaves are difficult to estimate due to the relatively limited volume of the rock material coming from the drill cores. The enclaves consist of 35–60 vol% plagioclase, 15–30 vol% biotite, 0–30 vol% pyroxene and 0–25 vol% amphibole. Quartz and K-feldspar are interstitial and subordinate. The accessory minerals include common magnetite and ilmenite, prismatic apatite, euhedral zircon and titanite. Monazite, allanite and chevkinite-group minerals are also present but less common. Texturally the enclaves can be classified mainly into three types: (1) fine-grained, melanocratic enclaves, and (2) medium-grained, mesocratic enclaves with equigranular (Fig. 3B) or porphyritic texture due to the presence of 0.5–2 cm-long feldspar phenocrysts (Fig. 3B, C). The last type (3) is represented by finer-grained, melanocratic enclaves, which display a magmatic flow texture (Figs. 2A and 3D) defined by mafic minerals and/or plagioclase crystals. This type of the enclaves also displays porphyritic texture caused by the presence of feldspar phenocrysts. No specific mineralogy can be attached to the particular types of enclaves.

The contact between the enclaves and granitoid host rocks is sharp (Fig. 2B, E) or partly diffuse (Fig. 2A, C, G). Occasionally, the contact between the granitoid and enclave is underlined by a visible decrease in the granitoid grain size (Fig. 2F) or by thin felsic haloes (enriched in quartz and K-feldspar) developed in the granitoid part (Fig. 2B). Some contacts are underlined by the presence of mafic minerals (biotite and amphibole; Figs. 2E, G and 3D). Rarely, large feldspar phenocrysts (up to 3 cm long) are observed to cross the contacts between the enclave and granitoid, or occur

within the enclaves (Figs. 2C, D, H and 3E). Plagioclase phenocrysts are characterized by the presence of numerous pyroxene, biotite, ilmenite and apatite inclusions. In the case of K-feldspar, plagioclase inclusions are also noticed (Fig. 3E). Generally, alkali feldspar phenocrysts are larger than plagioclase phenocrysts and show stronger signs of resorption. Most plagioclase phenocrysts are markedly rounded.

## Mineral compositions

### Feldspars

The plagioclase composition is given in Table S1 in the electronic supplementary material (ESM). The plagioclase grains from the granitoid are euhedral to subhedral, mostly with normal compositional zoning from andesine (max An<sub>46</sub>) to oligoclase (An<sub>29</sub>). The Or content reaches up to 4 mol% but it is usually around 2 mol%. Plagioclase associated with ilmenite-magnetite aggregates is solely albite (Ab<sub>95</sub>–Ab<sub>98</sub>).

In the enclaves, matrix andesine (An<sub>31</sub>–An<sub>42</sub>) grains are subhedral to anhedral, with uniform grain size and normal zoning. The plagioclase phenocrysts are euhedral to subhedral and show a composition of An<sub>41</sub>–An<sub>31</sub>. Crystals show poikilitic rims, mainly with pyroxene (classified as diopside) and ilmenite inclusions.

Both, subhedral alkali feldspar from granitoid rocks and alkali feldspar phenocrysts from enclaves display recurrent zoning with Or contents of 82–96 and 74–94 mol%, respectively (Table S2 in the ESM). Additionally, alkali feldspar phenocrysts from the enclaves often show poikilitic rims with inclusions of subhedral plagioclase (of constant composition An<sub>37–38</sub>), pyroxene (diopside), biotite (phlogopite), zoned apatite and ilmenite.

### Biotite

Biotite is classified as phlogopite, both within the granitoid rocks and enclaves (Table S3 in the ESM). It exhibits high and rather restricted Fe<sup>2+</sup>/(Fe<sup>2+</sup> + Mg) ratios of 0.43–0.48 (granitoid rocks) and 0.40–0.47 (enclaves). Phlogopite from the granitoids contains 0.83 to 1.84 wt% F and it has a high Ti content of 3.81–4.73 wt% TiO<sub>2</sub>.



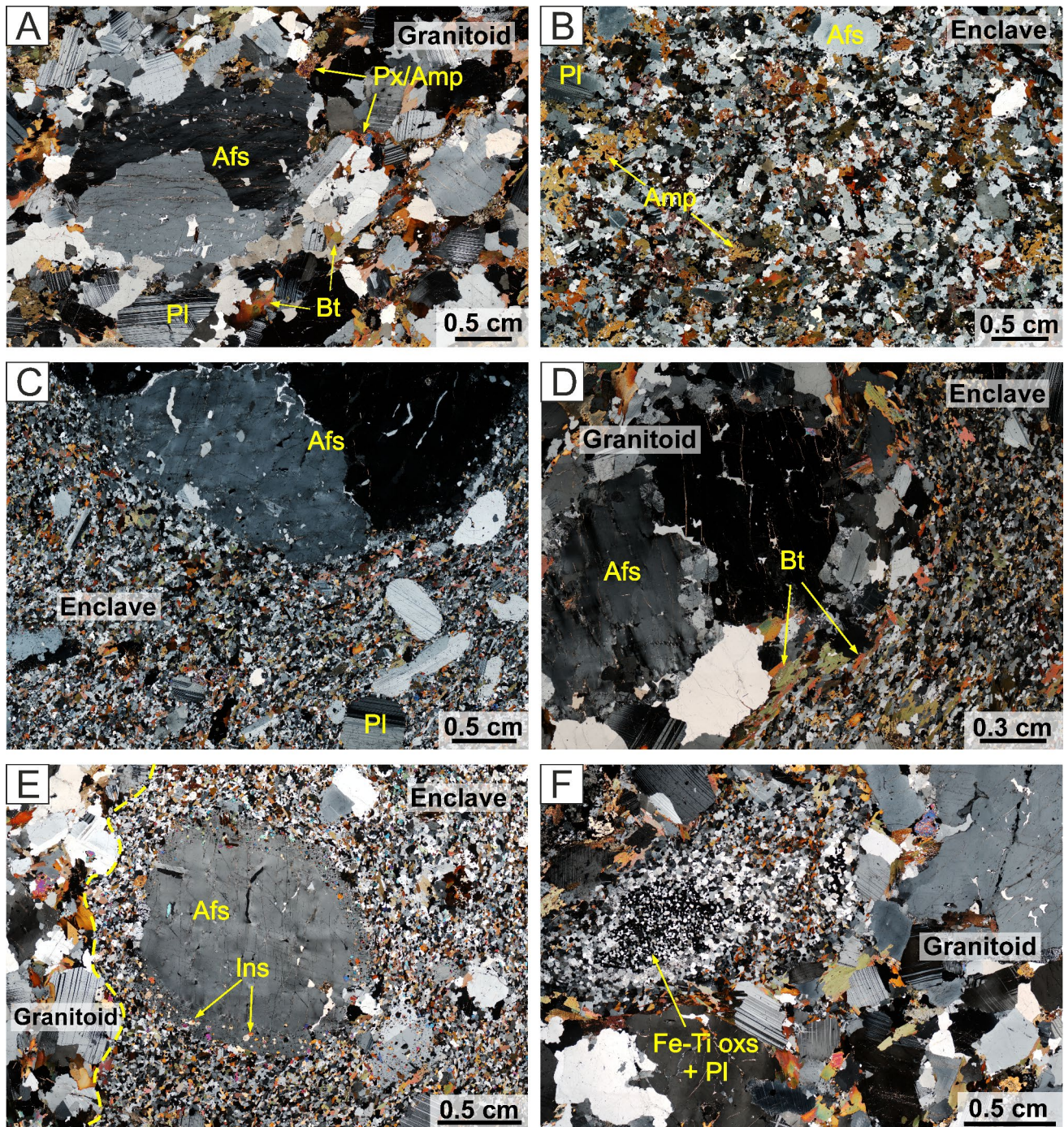


**Fig. 3** Cross-polarised transmitted-light images of enclaves: **A** coarse-grained texture of the granitoid rocks; **B** fine-grained texture of the enclave with single phenocrysts of feldspar; **C** contact between the enclave and granitoid host with feldspar phenocrysts; **D** contact between the enclave and granitoid host underline by the presence of

mafic minerals (biotite); **E** feldspar phenocrysts with rim of numerous inclusions within the fine-grained enclave; **F** diffusive contact between the enclave and granitoid host. Afs – alkali feldspar, Amp – amphibole, Bt – biotite, Fe-Ti oxs – Fe-Ti oxides, Ins – inclusions, Pl – plagioclase

Similar concentrations are shown by phlogopite from the enclaves: 0.86–1.93 wt% F and 3.19–4.70 wt% TiO<sub>2</sub>. The biotite grains are fresh with no signs of chloritization. Biotite commonly contains abundant zoned apatite, ilmenite and zircon inclusions.

### Pyroxene

Pyroxene, from granitoid rocks and enclaves, is mostly subhedral to euhedral and partially replaced by amphibole. It is classified as diopside (Table S4 in the ESM),



with a diopside composition of  $Wo_{48-50} En_{33-37} Fs_{14-19}$  for the granitoid rocks and  $Wo_{43-51} En_{33-36} Fs_{12-24}$  for the enclaves. Diopside composition, with  $Wo_{48-50} En_{33-35} Fs_{15-18}$ , is characteristic also for pyroxene present as inclusion in porphyrocrysts of plagioclase within the granitoid rocks.

### Amphibole

Amphibole is a subordinate phase in the granitoids, however, in the enclaves, it may occur as a dominant constituent. In the granitoids unzoned amphibole exhibits a constant chemical composition of magnesio-hastingsite (Table S5 in the ESM), whereas in the enclaves it is mainly magnesio-hastingsite with single grains of pargasite-magnesio-hastingsite and magnesio-ferrihornblende. Amphibole in both rock types show the  $Mg/(Mg+Fe^{2+})$  ratio of 0.56–0.63, uniform  $Al_2O_3$  content of 9.28–10.69 wt% and low Ti concentrations in the range of 1.06–1.79 wt%  $TiO_2$ . The amphibole from the enclaves is of igneous origin indicated by Si values that do not exceed the 7.50 a.p.f.u. limit for igneous amphibole (Leake 1971) and by the  $^{IV}Al/^{VI}Al$  ratio greater than 3.3, characteristic of unaltered igneous calcareous amphibole (Fleet and Barnett 1978).

### Accessory minerals

The main accessory minerals are apatite, zircon, titanite, ilmenite and magnetite. Apatite, classified as fluorapatite, is euhedral and prismatic. It exhibits oscillatory zoning with  $Ce_2O_3$  contents ranging from 0.23 to 1.13 wt%. Zircon is present in biotite and hornblende. It shows oscillatory zoning, reflecting a heterogeneous distribution of trace elements during magmatic growth. The Zr/Hf ratios in zircon vary significantly between 70 and 124. Ilmenite and magnetite form complex oxy-exsolution intergrowths. Allanite-, monazite- and chevkinite-group minerals are subordinate. Chevkinite-group minerals are more abundant than allanite, and occur as inclusions in phenocrysts together with the oxides. The unaltered crystals are of perrierite-(Ce) composition (Nejbert et al. 2020; Domańska-Siuda et al. 2022).

### Geochemistry

The  $SiO_2$  content in the granitoids ranges from 55.6 to 62.1 wt%. The rocks are chemically classified as monzonite, quartz monzonite and monzodiorite (Fig. 4A; Table 1), however, petrographic observation points to monzonite and granodiorite variety (cf. Petrography section). The granitoids are metaluminous, with the molar A/CNK ratio ranging from 0.86 to 0.93 (Fig. 4B). The samples have elevated  $K_2O$  contents (3.52–5.52 wt%) and plot in the high-K field in the  $K_2O$  versus  $SiO_2$  diagram (Rickwood 1989; Fig. 4C). The subalkaline character of the granitic rocks is evident on the  $(Na_2O+K_2O)$  versus  $SiO_2$  diagram (Irvine and Baragar 1971; Fig. 4A). The  $Na_2O/K_2O$  ratio ranges between 0.46 and 0.80. Following the Frost's classification (Frost et al. 2001), samples are mostly alkali-calcic and ferroan (Fig. 4D, E). The  $FeO_t/(MgO+FeO_t)$  (where iron is expressed as total  $FeO$ ;  $FeO_t = FeO + 0.8998 Fe_2O_3$ ) values range from 0.79 to 0.82 (Fig. 4E). The granitoids display the typical characteristics of A-type granites (Whalen et al. 1987), i.e., high contents of Zr (up to 734 ppm), Nb (up to 26 ppm), Ga (up to 23 ppm) and total REEs (up to 557 ppm). In the Zr versus  $10000 \times Ga/Al$  (Fig. 4F) and  $FeO_t/MgO$  versus  $Zr+Nb+Ce+Y$  (Fig. 4G) diagrams (Whalen et al. 1987) all the analyzed samples plot in the A-type granite field, whilst the Nb-Y-Ce triangular plot (Eby 1992) indicate the  $A_2$ -subtype affinity (i.e., anorogenic granite related to average continental crust or arc-type sources) of the studied granitoids (Fig. 4H).

The enclaves have a broad compositional range, with  $SiO_2$  contents varying from 45.5 to 58.8 wt% (Table 1) and exhibit mafic to intermediate composition of monzogabbro, monzodiorite and monzonite (Fig. 4A). The enclaves are metaluminous, with the A/CNK ratio between 0.65 and 0.83 (Fig. 4B). The  $FeO_t/(MgO+FeO_t)$  ratio is similar to those of the granitoid rocks (0.76–0.83), while the  $Na_2O/K_2O$  ratio is higher and ranges between 0.67 and 1.68. Generally, the enclaves plot in the field of alkali-calcic and ferroan rocks (Frost et al. 2001; Fig. 4D, E). Samples with a lower  $SiO_2$  content plot in the alkaline field, whereas the enclaves richer in silica have a sub-alkaline composition (Fig. 4A).

In the Harker diagrams, there is no visible chemical gap between the granitoid rocks and the enclaves (Figs. 5 and 4A,

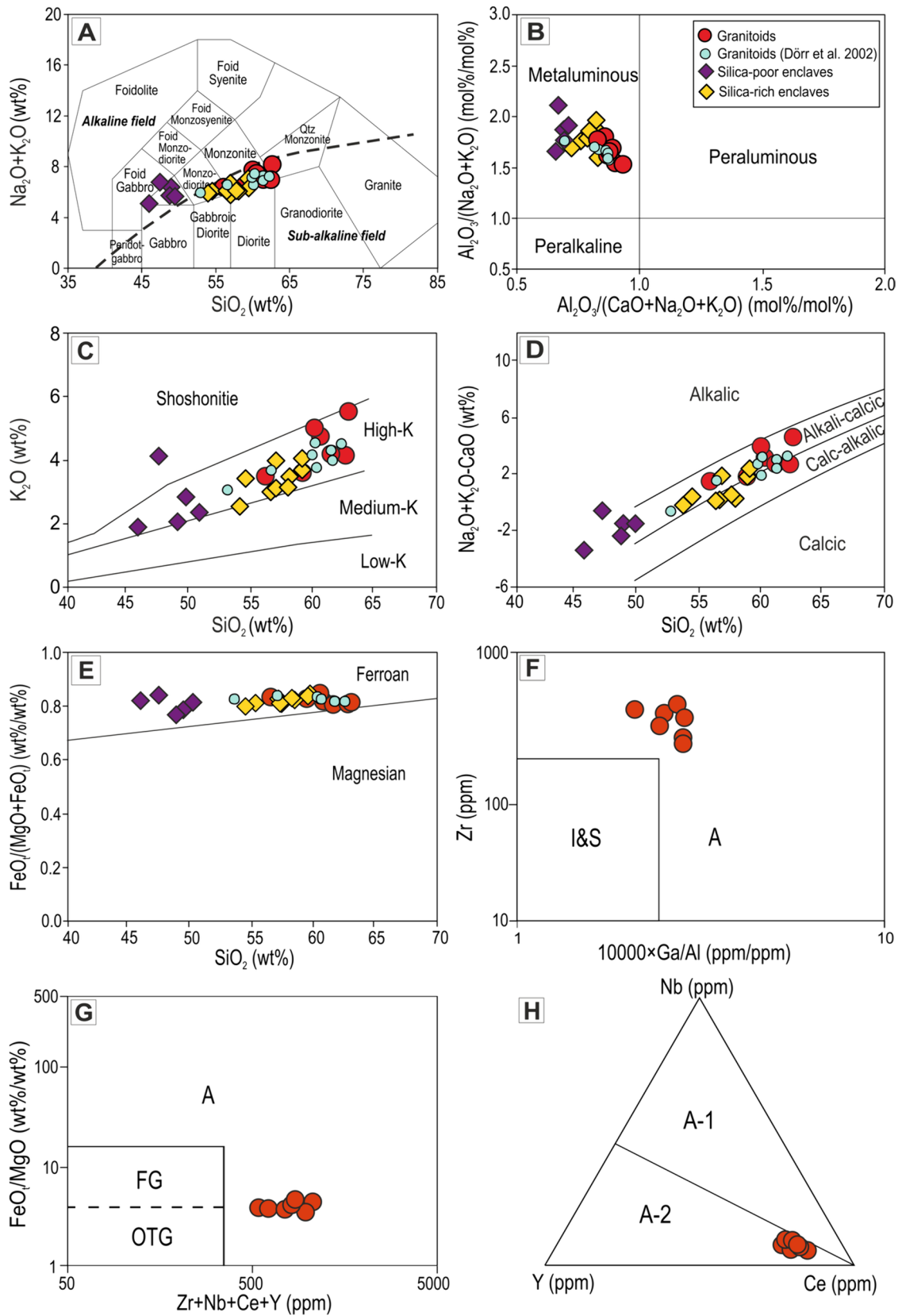




**Fig. 4** Discrimination diagrams for the Krasnopol PIG-6 borehole granitoid rocks and enclaves: **A**  $(\text{Na}_2\text{O}+\text{K}_2\text{O})$  versus  $\text{SiO}_2$  diagram (after Irvine and Baragar 1971); **B**  $\text{Al}_2\text{O}_3/(\text{Na}_2\text{O}+\text{K}_2\text{O})$  versus  $\text{Al}_2\text{O}_3/(\text{CaO}+\text{Na}_2\text{O}+\text{K}_2\text{O})$  molar diagram (after Shand 1943); **C**  $\text{K}_2\text{O}$  versus  $\text{SiO}_2$  diagram (after Rickwood 1989); **D**  $(\text{Na}_2\text{O}+\text{K}_2\text{O}-\text{CaO})$  versus  $\text{SiO}_2$  diagram (after Frost et al. 2001); **E**  $\text{FeO}_t/(\text{MgO}+\text{FeO}_t)$  versus  $\text{SiO}_2$  diagram (after Frost et al. 2001); **F** Zr versus  $10000^x\text{Ga}/\text{Al}$  diagram and **G**  $\text{FeO}_t/\text{MgO}$  versus  $\text{Zr}+\text{Nb}+\text{Ce}+\text{Y}$  diagram (after Whalen et al. 1987); A, I, and S refer to A-type, I-type, and S-type granite, FG – fractional granites, OTG – non-fractional granites; H: Nb–Y–Ce discrimination diagram for  $\text{A}_1$ - and  $\text{A}_2$ -type granites (after Eby 1992). The  $\text{A}_1$ -type represents within-plate granites, while the  $\text{A}_2$ -type represents post-collision granites. Data for other Krasnopol PIG-6 borehole granitoid results are from Dörr et al. (2002)

C–E). However, a division of the enclaves into two groups is evident: the first with a low  $\text{SiO}_2$  content (i.e., silica-poor enclaves with 45–50 wt%  $\text{SiO}_2$ ) and the second, enriched in silica (i.e., silica-rich with  $\text{SiO}_2$  ranging from 54 to 60 wt%). The silica-rich enclaves overlap with the granitoid samples. The silica-poor enclaves include the texturally distinguished type 1, while the silica-rich enclaves include types 2 and 3 (cf. Petrography section). A common trend of melt evolution over a wide range of silica content is evident for most elements (e.g., Fe, Mg, Ca, Ti, Co, Nb, Y and Sr). The Harker variation diagrams (Fig. 5) show negatively correlated trends for  $\text{TiO}_2$ ,  $\text{Fe}_2\text{O}_3$ , MgO, CaO, Nb, Nd and Y, V, Ta, REEs (except Eu, not shown) against  $\text{SiO}_2$ . Plots of  $\text{K}_2\text{O}$ , Rb and Ba (not shown) against  $\text{SiO}_2$  exhibit positively correlated trends.  $\text{Al}_2\text{O}_3$ ,  $\text{Na}_2\text{O}$  (not shown), Sr, Eu and Ga (not shown) remain relatively constant with increasing  $\text{SiO}_2$ . There is some scatter in the data set, i.e., for Zr and Hf (not shown). In the case of the enclaves, the Th content remains constant with increasing  $\text{SiO}_2$ , while granitoids show data dispersion.

Chondrite-normalized (Nakamura 1974) rare earth element patterns for the granitoids and enclaves are shown in Fig. 6. The total REE concentrations in the granitoids are in the range of 371–557 ppm (Table 1). The patterns for the granitoid rocks are homogenous, showing the uniform REE distribution (Fig. 7A) with relatively steep patterns for light rare earth elements [LREEs;  $(\text{La}/\text{Sm})_N = 3.7\text{--}5.0$ ; where N is chondrite (C1) normalized to values of Nakamura (1974)] and moderately steep for high rare earth elements [HREEs;  $(\text{Gd}/\text{Yb})_N = 2.3\text{--}3.0$ ], giving well-defined fractionation trends [ $(\text{La}/\text{Yb})_N = 15.1\text{--}19.7$ ; Table 1]. The majority of samples display negative Eu anomalies, i.e.,  $\text{Eu}/\text{Eu}^* = 0.66\text{--}0.84$ , except one sample with a slightly positive Eu anomaly of 1.05.

The enclaves show uniform REE patterns for both groups (Fig. 6C). The silica-poor enclaves have high total REE contents ranging from 625 to 752 ppm. The chondrite-normalized patterns are markedly LREE-enriched, with moderately steep LREE [ $(\text{La}/\text{Sm})_N = 2.9\text{--}3.4$ ] and HREE patterns [ $(\text{Gd}/\text{Yb})_N = 2.4\text{--}2.6$ ;  $(\text{La}/\text{Yb})_N = 10.6\text{--}13.3$ ], and negative Eu anomalies ( $\text{Eu}/\text{Eu}^* = 0.51\text{--}0.56$ ). The silica-rich enclaves have lower total REE contents (358–626 ppm) and less pronounced Eu anomalies ( $\text{Eu}/\text{Eu}^* = 0.67\text{--}0.92$ ) than the more mafic varieties. The silica-rich enclaves show enrichment in LREEs [ $(\text{La}/\text{Sm})_N = 3.1\text{--}4.1$  and  $(\text{La}/\text{Yb})_N = 12.3\text{--}25.6$ ] with moderately steep HREE patterns [ $(\text{Gd}/\text{Yb})_N = 2.3\text{--}2.7$ ]. Compared to the granitoid host rocks, all enclaves have slightly higher HREE concentrations.

Trace element signatures are presented in normal mid-ocean ridge basalt (N-MORB) normalized (Sun and McDonough 1989) multi-element diagrams (Fig. 6B, D). All rocks are enriched in large ion lithophile elements (LILE) compared to N-MORB. The granitoids exhibit homogenous patterns, with negative anomalies for U, Nb, Sr, P, and Ti (Fig. 6B). The trace element patterns of the silica-rich enclaves (Fig. 6D) are similar to the granitoid patterns except for much stronger negative U anomalies in the enclaves. The silica-poor enclaves (Fig. 6D) exhibit enrichment in HREE, as well as negative U, Sr, Ti and no P anomalies compared to granitoid samples.

### Sr–Nd isotope data

The Sr–Nd isotope compositions of three host granitoids and four enclave samples are given in Table 2. The U–Pb zircon age of  $1507 \pm 6$  Ma (Wiszniewska and Krzemińska 2021) of the granitoid rocks was used to calculate the initial  $^{87}\text{Sr}/^{86}\text{Sr}$  ratios and  $\epsilon_{\text{Nd}}(1507)$  values.

The granitoid samples have relatively high Rb and Sr concentrations of 114.0–129.5 ppm and 363.8–383.1 ppm, respectively. The initial  $^{87}\text{Sr}/^{86}\text{Sr}$  values range from 0.7084 to 0.7138 and  $^{87}\text{Rb}/^{86}\text{Sr}$  from 0.86 to 0.99. The enclaves show comparable to granitoids Sr concentrations of 352.4–396.3 ppm, but lower Rb contents of 73.9–94.9 ppm. The initial  $^{87}\text{Sr}/^{86}\text{Sr}$  values fall between 0.7052 and 0.7075, and the  $^{87}\text{Rb}/^{86}\text{Sr}$  ratio changes from 0.56 to 0.70. The difference between the two rock types is also visible in the Sm and Nd concentrations. In the case of the granitoids, the measured Nd and Sm concentrations vary from 63.8 to 122.4 ppm for Nd and from 10.6 to 20.5 ppm for Sm, whereas the enclaves exhibit Nd content of 95.6–152.6 ppm and Sm of 17.0–27.4 ppm. The initial  $\epsilon_{\text{Nd}}$

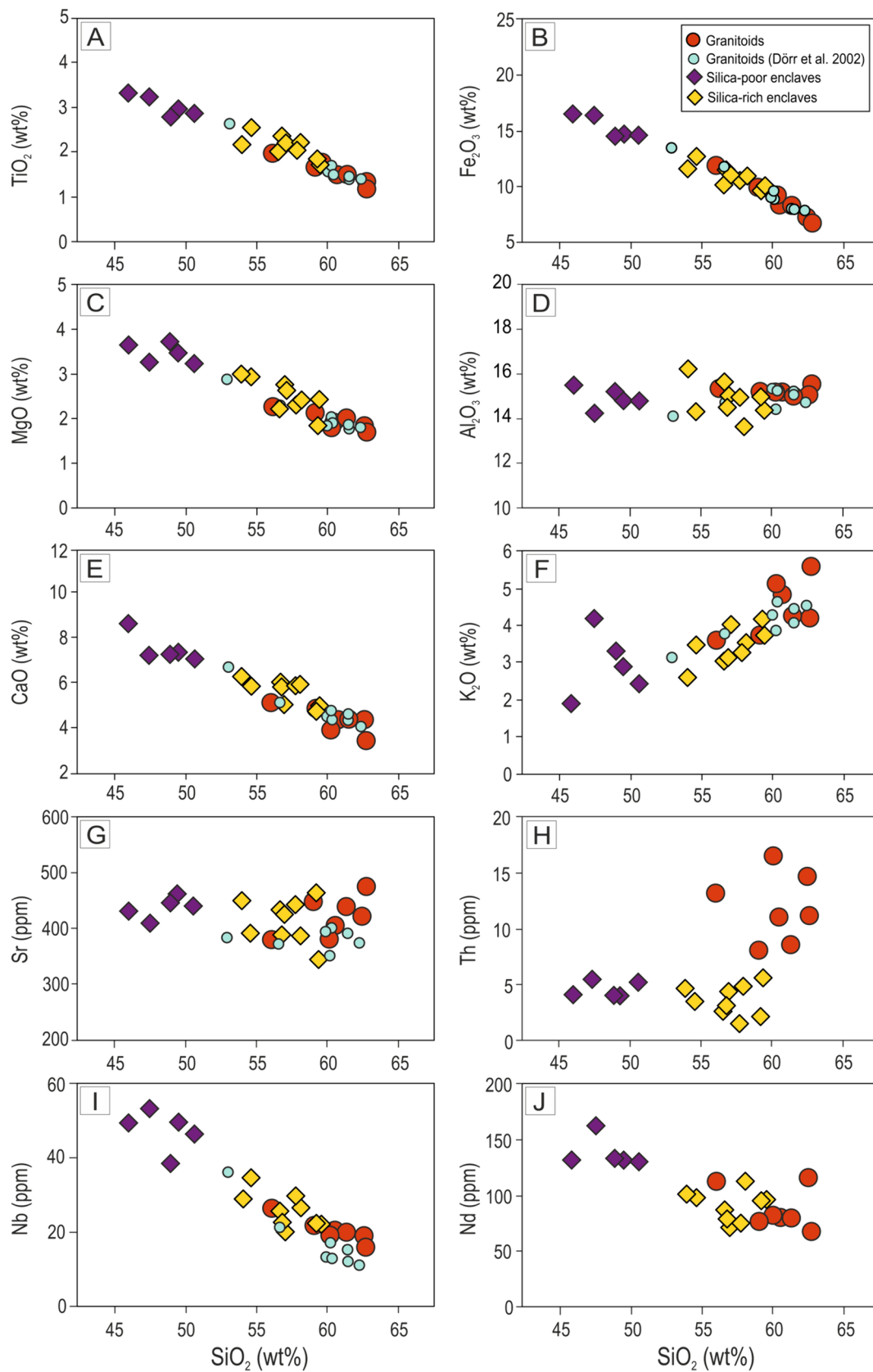


**Fig. 5** Selected variation of major and trace element compositions versus silica (wt%) for whole-rock samples of the Krasnopol FIG-6 borehole granitoid rocks and enclaves. Data for other Krasnopol FIG-6 borehole granitoid results are from Dörr et al. (2002)

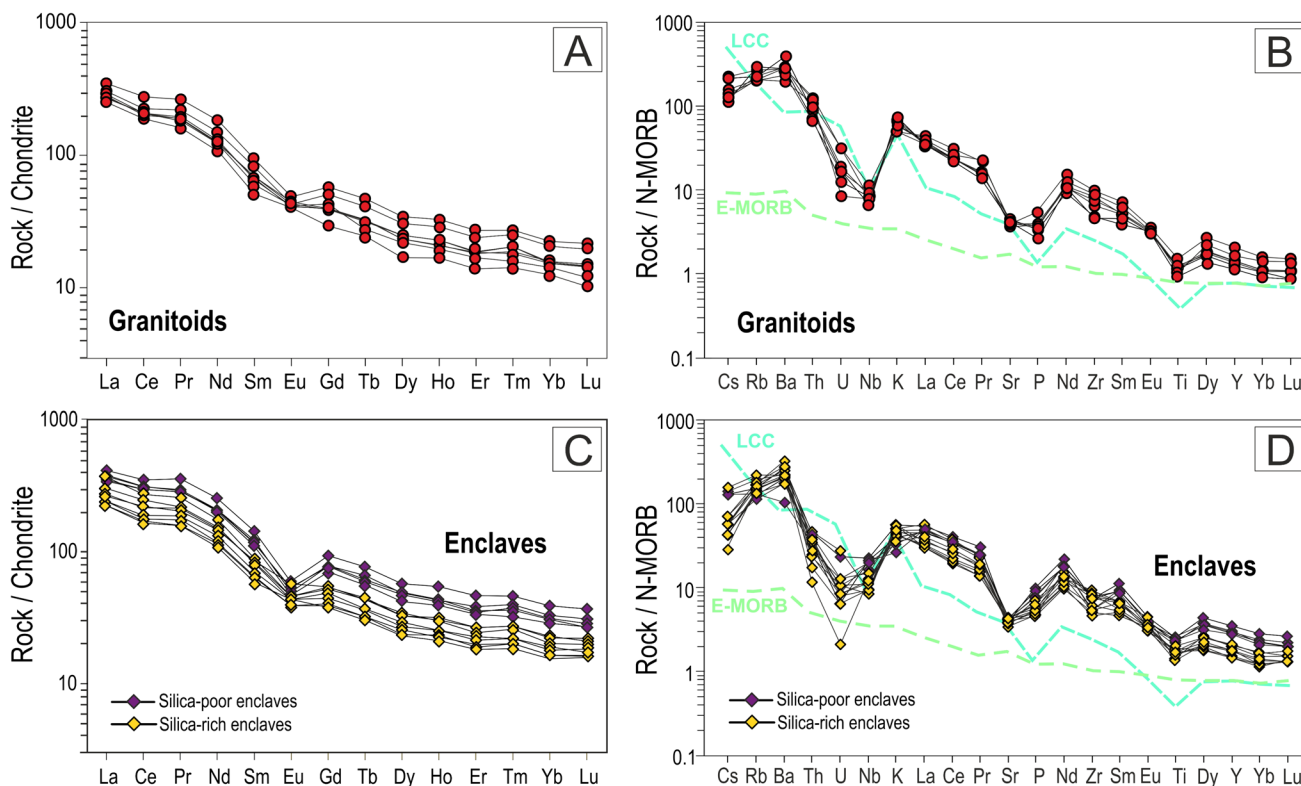


**Fig. 6** Chondrite-normalized (Nakamura 1974) rare-earth element patterns for **A** granitoids and **C** enclaves; Normal mid-ocean ridge basalt (N-MORB) normalized (Sun and McDonough 1989) trace

element patterns for the **B** granitoids and **C** enclaves. Average of lower continental crust (LCC) and enriched mid-ocean ridge basalt (E-MORB) are from (Sun and McDonough 1989)

values fall at -3.8 to -4.0 for the granitoids and show a slightly wider range of -2.6 to -3.8 for the enclaves. Corresponding  $T_{DM}$  model ages following the model of DePaolo (1983) fall at

2.09 and 2.10 Ga for the granitoids and from 2.05 to 2.11 Ga for the enclaves (Fig. 7). The isotopic characteristics do not show any obvious correlation between Nd and Sr isotope values and  $SiO_2$  content (not shown).

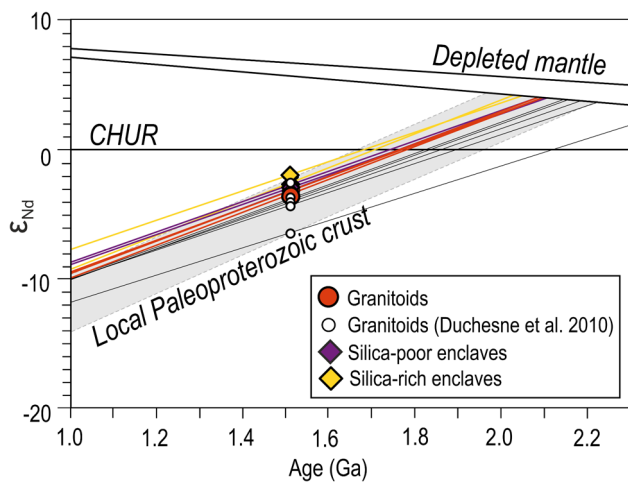


**Fig. 7** Epsilon-Nd versus age diagram showing evolution lines for the Krasnopol PIG-6 borehole granitoid rocks and enclaves. The Krasnopol data are shown in comparison with the local Paleoproterozoic crust evolution array. Data for Paleoproterozoic samples are from Krzemińska et al. (2017). Data for the Mazury granitoids are from Duchesne et al. (2010). The depleted mantle curve is from DePaolo (1981)

**Crystallization conditions**

The mineral chemical compositions were used to determine the crystallization p-T conditions. The geothermobarometric calculations are shown in Table 3.

The temperature estimations were based on the Ti-in-amphibole calibration by Otten (1984), the Ti-in-biotite thermometer of Henry et al. (2005), the zircon saturation temperature of Crisp and Berry (2022) and the clinopyroxene-liquid thermometers of Putirka (2008). The Al-in-amphibole geobarometer by Mutch et al. (2016) and Anderson and Smith (1995) were used for pressure evaluation.

The calculated pressures for calcic amphibole (Mutch et al. 2016) range from 4.2 to 4.6 kbar (mean = 4.5 kbar) for the granitoid samples and from 3.7 to 4.6 kbar (mean = 4.3 kbar) for the enclaves. The estimated amphibole temperature (Otten 1984), is within the range of 747–783 °C (mean = 758 °C) for the granitoids and

**Table 2** Sm-Nd and Rb-Sr isotopic results of the granitoid rocks and magmatic microgranular enclaves from the Krasnopol PIG 6 borehole

Sample	KR-6-3	KR-6-50G	KR-6-31	KR-6-37	KR-6-48	KR-6-35	KR-6-54
Lithology	GR	GR	GR	SP-ME	SP-ME	SR-ME	SR-ME
Sm* (ppm)	10.56	20.52	16.03	26.17	27.40	17.04	17.55
Nd* (ppm)	63.79	122.36	93.90	146.66	152.56	101.22	95.55
$^{147}\text{Sm}/^{144}\text{Nd}$	0.1001	0.1014	0.1032	0.1079	0.1085	0.1018	0.1110
$\text{Nd}/^{144}\text{Nd}_m$	0.511477	0.511502	0.511519	0.511589	0.511583	0.511506	0.511657
$^{143}\text{Nd}/^{144}\text{Nd}_t$	0.510486	0.510498	0.510497	0.510521	0.510508	0.510498	0.510558
$\text{ENd}_{(0)}$	-22.6	-22.2	-21.8	-20.5	-20.6	-22.1	-19.1
$\text{ENd}_{(t)}^a$	-4.0	-3.8	-3.8	-3.3	-3.6	-3.8	-2.6
$T_{DM}(\text{Ga})^b$	2.10	2.09	2.10	2.09	2.11	2.09	2.05
Rb (ppm)	129.5	116.0	114.0	73.9	85.4	74.4	94.9
Sr (ppm)	377.6	363.8	383.1	373.5	352.4	384.9	396.3
$^{87}\text{Rb}/^{86}\text{Sr}$	0.9948	0.9249	0.8626	0.5731	0.7020	0.5598	0.6938
$^{87}\text{Sr}/^{86}\text{Sr}_m$	0.73374	0.73343	0.72680	0.71974	0.72017	0.71818	0.72176
$^{87}\text{Sr}/^{86}\text{Sr}_t$	0.71257	0.71375	0.70844	0.70754	0.70523	0.70627	0.70700
$\text{ESr}_{(0)}$	415	411	316	216	222	194	245
$\text{ESr}_{(t)}$	140	157	81	68	35	50	61

GR granitoid, SP-ME silica-poor enclave, SR-ME silica-rich enclave, *m* measured, *t* time (1507 Ma)

\*Sm and Nd concentrations were determined by isotope dilution

<sup>a</sup> $\text{eNd}(t)$  values were calculated using  $^{143}\text{Nd}/^{144}\text{Nd}=0.512638$  and  $^{147}\text{Sm}/^{144}\text{Nd}=0.1967$  in the present (0) chondrite (Jacobsen and Wasserburg 1980), <sup>b</sup> $T_{DM}$  depleted mantle Nd model age

690–792 °C (mean = 741 °C) for the enclaves. When the temperature is taken into account, the pressure calculated for amphibole in granitoids ranges from 4.1 to 4.7 kbar (mean = 4.3 kbar; Anderson and Smith 1995), while for the enclaves it ranges from 4.1 to 5.2 kbar (mean = 4.5 kbar). The temperatures obtained on biotite (Henry et al. 2005) range from 626 to 661 °C for the granitoids, and from 594 to 658 °C for the enclaves. The equation derived from the experimental data of Crisp and Berry (2022) on the solubility of zircon in melts with various basinity can be used as a geothermometer. When the pressure (mean = 4.4 kbar) and H<sub>2</sub>O content of the melt (5%) are

taken into account, zircon saturation temperatures for the studied granitoids range from 790 to 850 °C and vary over a wide range from 687 to 823 °C for the enclaves. The highest temperatures of 980–1041 °C (mean = 1005 °C) for granitoids and 1026–1097 °C (mean = 1063 °C) for enclaves were provided by the clinopyroxene–liquid thermometers (Putirka 2008).

The presence of magnetite in the granitoid mineral assemblages, the high whole-rock (wt%) ratios of FeO<sub>t</sub>/(FeO<sub>t</sub> + MgO) (with an average of 0.80; Anderson and Morrison 2005) and the presence of magmatic amphiboles with low Fe# values [Fe# = Fe/(Fe+Mg) mole, 0.40–0.43], correspond to high oxygen fugacity conditions (Fe# < 0.6; Anderson and Smith 1995). The same oxidized character was previously reported for other hornblende-bearing granitoid intrusions from the Mazury Complex (Duchesne et al. 2010).

Oxidized A-type granites are considered to crystallize from magmas with appreciable water contents. The H<sub>2</sub>O content of the melt, estimated using the method of Ridolfi et al. (2010), is approximately 5% by weight for both granitoids and enclaves. This is consistent with experimental studies by Clemens et al. (1986), Dall'Agnol et al. (1999), Bogaerts et al. (2006) and Dall'Agnol and de Oliveira (2007), which indicate wet (5–6 wt% H<sub>2</sub>O) and oxidized magmas (oxygen fugacity NNO+1) as the parental magmas for rapakivi-like A-type granites.

**Table 3** Geothermobarometric calculation results for the granitoid rocks and magmatic microgranular enclaves from the Krasnopol PIG 6 borehole

Lithology	GR	ME
P (kbar)		
Al-in-hornblende (Mutch et al. 2016)	4.2–4.6	3.7–4.6
Al-in-hornblende (Anderson and Smith 1995)	4.1–4.7	4.1–5.2
T (°C)		
Ti-in-biotite (Henry et al. 2005)	626–661	594–658
Ti-in-amphibole (Otten 1984)	747–783	690–792
Zircon saturation (Crisp and Berry 2022)	790–850	687–828
Clinopyroxene–liquid (Putirka 2008)	980–1041	1026–1097

GR granitoid, ME enclave



## Discussion

### Petrogenesis of microgranular enclaves

#### Generalities

Many mechanisms have been proposed for the genesis of the dark, microgranular enclaves ((Didier 1973; Fershtater and Borodina 1977, 1991; Vernon 1984, 1991; Chappell et al. 1987; Chappell and White 1991; Castro et al. 1990; Barbarin and Didier 1991; Reid et al. 1993; Elburg 1996; Dorais et al. 1997; Collins et al. 2000; Donaire et al. 2005; Kumar and Rino 2006; Słaby and Martin 2008; Shellnutt et al. 2010; Perugini and Poli 2012; Flood and Shaw 2014; Chen et al. 2015; Kumar 2020, and others)). The data obtained in this contribution have been used to provide the best model for the origin of microgranular enclaves in the A-type Krasnopol granitoid intrusion.

#### Restite model

The ‘restite model’ assumes that the enclaves represent the solid residues of refractory minerals after the partial melting of the granitoid source rocks. Such enclaves should have metamorphic or residual sedimentary textures inherited from the source. However, the examined enclaves do not show such features. The enclaves display igneous textures, i.e., euhedral crystals of feldspars, elongate, lath-like crystals of feldspars and biotite in the groundmass (without internal deformation; Fig. 3D), inclusions of quartz and feldspars in other minerals. The Krasnopol enclaves show evidence of magma interaction, manifested by the presence of common partly melted crystals (Fig. 3C, E) derived from earlier stages of the same magma system (antecrysts) or from mixing with other magma batches (xenocrysts). Such features suggest magmatic crystallization (Didier 1984). In addition, restite enclaves should be enriched in Al-rich minerals (i.e., andalusite, sillimanite, cordierite, corundum, spinel), which are not observed in the Krasnopol enclaves. The Krasnopol enclaves have a similar to granitoids phase assemblage, but with a higher ratio of mafic minerals, i.e., biotite, amphibole and clinopyroxene, and overlapping mineral chemical compositions (Tables S1–S5). Moreover, the composition of amphibole in the enclaves, i.e., the Si values < 6.63 and the  $^{IV}Al/^{VI}Al$  ratio over 3.3, support its magmatic origin (Fleet and Barnett 1978). The restite model is ruled out also by the whole-rock geochemical data. The enclaves have high REEs (slightly higher REE sum than the host granitoids) and trace elements abundances (Fig. 6C, D; Table 1). Enclaves of restite origin are mostly found within S-type granitoids (of sedimentary protoliths), which are generally peraluminous. This is contrary

to the A-type Krasnopol granitoids being of metaluminous character (Fig. 4B). Hence, a restite model for the investigated enclaves can be excluded.

#### Autolith versus magma mixing models

The autolith and magma mixing models assume an igneous origin of the enclaves (see Introduction and references therein). The first model treats enclaves as ‘cumulates’ or ‘autoliths’ formed due to fractional crystallization. The term ‘autoliths’ is used to emphasize the cognate nature of the enclaves and the host granitoids. The second model assumes that the enclaves represent the coeval mafic magmas, which intruded into the felsic melts, mingled and quenched as ‘globules’ or ‘blobs’ due to high viscosity and temperature contrast.

In the Harker diagrams (Fig. 5), the majority of elements (e.g., Fe, Mg, Ca, Ti, Co, Nb, Y and Sr) show a chemical continuity from the enclaves to the granitoid host rocks with a gap between 50–54 wt% SiO<sub>2</sub> showing two groups of the enclaves. These well-defined linear trends suggest that both fractional crystallization and magma mixing-mingling may be the main processes, which influenced the chemical composition of the Krasnopol enclaves.

The autolith model assumes that the enclaves represent early crystallized cumulus phases or more mafic cogenetic fractions with trapped interstitial melts. The microgranular texture of the enclaves can be explained by the rapid cooling of magma at the marginal part of the magma chamber or the margins of magma conduits. Such conditions cause rapid crystallization of ferromagnesian minerals (Naney and Swanson 1980), particularly biotite, pyroxene and amphibole (Donaire et al. 2005). However, the studied enclaves do not reveal significant concentrations of biotite. The xenomorphic morphology of biotite indicates its crystallization after plagioclase and clinopyroxene. The few millimeters thick biotite aggregates, if present, occur only along the borders of some enclaves with the host rock (Figs. 2E, G and 3D). Concurrently, amphibole is a secondary phase after pyroxene. The petrographic observations are in accord with the estimated temperatures (Table 3). The temperatures of ca. 1000 °C for pyroxene in granitoids and 1060 °C for pyroxene in enclaves (clinopyroxene–liquid thermometers; Putirka (2008)), confirm that clinopyroxene and plagioclase are the earliest crystallizing phases. On the other hand, the low zircon saturation temperatures (around 810 °C) are similar to those obtained for amphibole. Therefore, zircon and amphibole are relatively late. Biotite is the last crystallizing phase, which is indicated by its xenomorphic morphology and temperatures close to 645 °C.

In addition, enclaves of cumulus (autolithic) origin are depleted in REEs and incompatible elements and exhibit positive Eu anomalies as compared to cogenetic evolved

melts. However, the silica-poor Krasnopol enclaves (45–50 wt% SiO<sub>2</sub>) show the opposite tendency, i.e., they are enriched in REEs and show more pronounced negative Eu anomalies (0.51–0.92) than their host rocks (0.66–1.05; Fig. 6C). REEs of silica-rich enclaves (54–60 wt% SiO<sub>2</sub>) overlap with the granitoids (Fig. 6A, C). Furthermore, the Krasnopol enclaves are abundant in most trace elements (except Rb, Ba, Th) in relation to granitoid rocks (Fig. 6C, D).

The cogenetic origin of the enclaves and host granitoids is not evident by Sr–Nd isotopes, which differ somewhat between two rock types. The <sup>87</sup>Sr/<sup>86</sup>Sr isotope ratio shows distinct nature of the enclaves and granitoids. The granitoid <sup>87</sup>Sr/<sup>86</sup>Sr initial values range from 0.7084 to 0.7138, while the enclaves show lower values between 0.7052 and 0.70754 (Table 2). The <sup>87</sup>Rb/<sup>86</sup>Sr isotope ratio ranges from 0.86–0.99 for the granitoids, and 0.56–0.70 for the enclaves indicating that the granitoids originate from a more radiogenic source. The slight difference between the two rock types is also visible in the εNd<sub>(1507)</sub> values, i.e., granitoids show a narrow range between -3.8 and -4.0, whereas enclaves display a slightly wider range from -2.6 to -3.8 (Table 2). To sum up, the geochemical and isotopic composition of the enclaves, as well as textural evidence argue against an autolith origin.

Macro- and micro-observations of relations between the granitoids and the enclaves suggest that the latter were incorporated into the host melt as more mafic magma globules. Initially rounded globules became elongated due to stretching within the partially crystallized, convective granitic magma body. The degree of elongation correlates with a direction of the mineral flow of the host granitoids (Figs. 2A, B and 3D, F), which points to the mutual nature of mafic and felsic magmas before their solidification (Vernon et al. 1988; Kumar et al. 2004). Differences in grain size of the enclaves and granitoids can be explained by a fast nucleation and crystal growth within the enclaves due to undercooling of mafic magma intruding into a cooler more Si-rich magma chamber (e.g., Vernon 1983).

The silica-rich enclaves textural (type 2 and 3) are mesocratic and compared to silica-poor enclaves (textural type 1) are characterized by higher plagioclase contents. The contact between the medium-grained enclaves (type 2) and the surrounding granitoids is gradational. The presence of partly diffuse/lobate contacts (Fig. 2A, C, D, H), indicates that mafic melts were still plastic when intruding into the host granitoids, whereas the formation of thin felsic haloes around the enclaves points to an interaction between more mafic (enclave) and felsic magmas (Fig. 2B). These haloes likely represent the so-called ‘bleaching’ zones of Vernon (1991). The silica-poor enclaves display sharp contact with

the granitoids (Fig. 2E–G). The concentration of mafic minerals, i.e., biotite and amphibole, at the margin of the enclaves (Figs. 2E, G and 3D), is most likely caused by the nucleation and subsequent fast growth of the mafic phases due to the rapid decrease in temperature of the mafic magma. The formation of biotite and amphibole as hydrous phases was possible due to selective diffusion of potassium and water, which was provided into the mafic melts from the K-saturated wet felsic component (Johnston and Wyllie 1988; Barbarin and Didier 1991; Wiebe 1994). This is confirmed by petrographic observations, i.e., the replacement of pyroxene by amphibole and crystallization of biotite as the latest phase. The single feldspar phenocrysts, which are observed within the enclaves and at the contact between the enclaves and host rocks (Figs. 2C, H and 3A, C, E, F), were most likely emplaced into the enclaves mechanically (Vernon 1984), and should be considered as an evidence of magma mingling (Barbarin and Didier 1991). Most feldspar phenocrysts are strongly rounded (Fig. 3C, E) and show stronger signs of resorption. The phenocrysts are characterized by abundant inclusions of mafic minerals (and plagioclase inclusions in the case of alkali feldspar phenocrysts) at the crystal margins (Fig. 3E), which is most likely the result of the attainment of chemical equilibrium between the plagioclase phenocrysts and mafic magma. Plagioclase and alkali feldspar oikocrysts in poikilitic texture suggest that mafic magma has cooled (solidified) along with host felsic melt (Fig. 3E, F; e.g., Vernon 1990; Hibbard 1991; Perugini et al. 2003).

### Geochemical modelling

The interaction between two melts may be responsible for the chemical variation in the enclaves especially in the silica-rich type. To show the effect of felsic-mafic magma interaction the mixing test of Fourcade and Allegre (1981) was applied. The following equation of the mass equilibrium law was used:

$$C_M^i = XC_A^i + (1 - X)C_B^i \quad (1)$$

where:  $C_M^i$  is the content of  $i$  element in hybrid melt;  $C_A^i$  is the content of  $i$  element in mafic melt;  $C_B^i$  is the content of  $i$  element in felsic melt and  $X$  is the mass fraction of the mafic component A in the hybrid melt M.

The assumption that the enclaves are hybrid rocks produced by the mixing of primary mafic and host felsic magmas was made. The enclave sample with the most primitive composition (Kr-6-37; 45.5 wt% SiO<sub>2</sub>) was used as representative of the mafic magma, which during the mixing with felsic melts (sample Kr-6-3; 62.1 wt% SiO<sub>2</sub>) produced

enclaves with a diverse  $\text{SiO}_2$  content. Accordingly, two mixing tests (Fig. 8A, B, Table 4) were carried out to obtain the hybrid composition of the enclave samples ( $C_{M1}$  - sample Kr-6-45,  $C_{M2}$  - sample Kr-6-42) with different silica content. The Kr-6-45 sample (49.1 wt%  $\text{SiO}_2$ ;  $C_{M1}$ ) and the Kr-6-42 sample (54.1 wt%  $\text{SiO}_2$ ;  $C_{M2}$ ) were chosen as representatives of the silica-poor and silica-rich enclaves, respectively. In terms of major oxides, the proportions of mafic component (X) are 0.79 (Kr-6-45 sample) and 0.51 (Kr-6-42 sample) in the hybrids and may explain the composition of the tested enclaves. The linear correlations are close to 1. The abundances of trace elements were also calculated for both samples based on the proportions of the mafic component (X) (e.g., Castro et al. 1990). The estimates are presented on N-MORB normalized (Sun and McDonough 1989) multi-element diagrams and compared to the actual values from the chemical analysis (Fig. 8C, D, Table 4).

The calculated and observed contents of Cs, Rb, U, P and Zr for the Kr-6-45 sample as well as Cs, Rb, Th, P and Zr for the Kr-6-42 sample do not match well. However, in both cases, the calculated REE contents are consistent with the REE compositions of the real enclave samples. Some trace elements, e.g., HFSE (Zr, Hf, Th), which do not fit the mixing test and do not easily exchange during the two-melt interaction process (Blundy and Wood 2003a, b), are mainly bound in accessory minerals, for instance in zircon (Zr, Hf), apatite (P), titanite

(Ti), Fe-Ti oxides (Ti) and chevkinite-group minerals (Nb, Ti). Therefore, the discrepancy in the concentrations of these elements could be a consequence of the mechanical sorting of HFSE-bearing accessories during differentiation and mixing, which leads to uneven distribution. Additionally, the experimental work of Perugini et al. (2006, 2008) demonstrated a strongly variable mobility of trace elements in the same mixing system. Thus, the partial modification of the enclaves and host rocks by late hydrothermal fluids may have triggered changes in the contents of mobile elements such as Rb and Cs. Concurrently, it should be stressed that the composition of the most mafic enclave (Kr-6-37) and most differentiated granitoid (Kr-6-3) used in the mixing calculations may not necessarily represent real mafic (enclave) and felsic magma end-members, respectively, unchanged by later processes.

The low Mg numbers [ $\text{Mg}\# = \text{Mg}/(\text{Mg} + \text{Fe}^{2+})$ ; 0.27–0.37], low Cr and Ni (below detection limit, Table 1), and high  $\text{TiO}_2$ ,  $\text{Fe}_2\text{O}_3$ ,  $\text{Al}_2\text{O}_3$ ,  $\text{P}_2\text{O}_5$ , and Zr contents (Table 1) of the enclaves suggest that they did not crystallize from primitive basaltic melts, but were generated from more evolved liquids with accumulations of plagioclase, hornblende, apatite, Fe-Ti oxides and zircon. This indicates that the mafic melts, from which the enclaves crystallized, had undergone previous fractionation or crustal contamination before they intruded into the host felsic magma chamber.

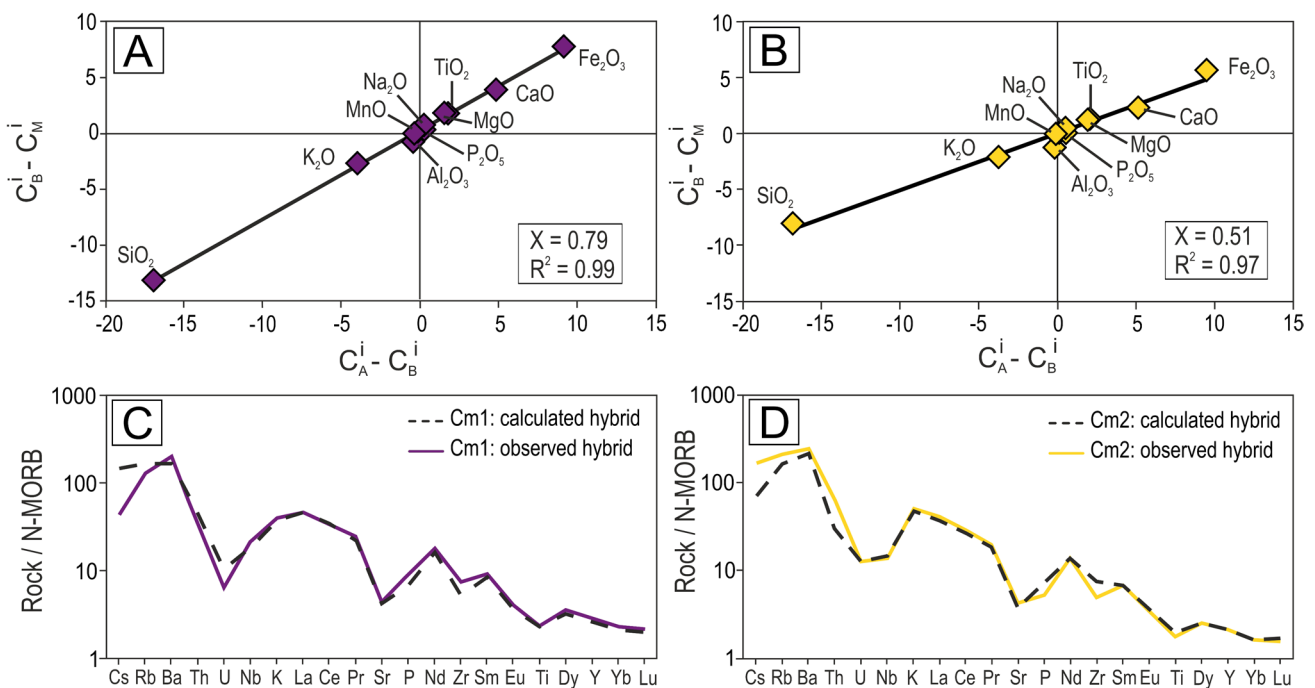


**Fig. 8** Major oxide mixing test (Fourcade and Allegre 1981) for hybrid enclave samples. **A** Kr-6-45 ( $C_{M1}$ ), **B** Kr-6-42 ( $C_{M2}$ ); Normal mid-ocean ridge basalt (N-MORB) normalized (Sun and McDonough 1989) calculated and observed trace element patterns for **C** Kr-6-45

( $C_{M1}$ ) and **D** Kr-6-42 ( $C_{M2}$ );  $C_A^i$  is content of  $i$  element in felsic melt;  $C_B^i$  is content of  $i$  element in mafic melt;  $C_M^i$  is content of  $i$  element in hybrid melt; X is the mass fraction of the mafic component B in the hybrid melt M;  $R^2$  = correlation coefficient

**Table 4** Concentrations of particular elements in the A, B magmas and the mixture M. Values normalized to 100%

Sample	KR-6-37 $C_A$	KR-6-3 $C_B$	KR-6-45 $C_{M1}$ observed	KR-6-42 $C_{M2}$ observed	$C_{M1^*}$ calculated	$C_{M2^{**}}$ calculated
Major oxides (wt %)						
SiO <sub>2</sub>	46.00	62.67	49.49	54.61	49.50	54.17
TiO <sub>2</sub>	3.33	1.18	2.99	2.54	2.88	2.27
Al <sub>2</sub> O <sub>3</sub>	15.46	15.54	14.80	14.29	15.47	15.50
Fe <sub>2</sub> O <sub>3t</sub>	16.43	6.88	14.68	12.60	14.42	11.75
MnO	0.32	0.11	0.30	0.22	0.28	0.22
MgO	3.67	1.65	3.45	2.92	3.25	2.68
CaO	8.76	3.54	7.46	5.89	7.66	6.20
Na <sub>2</sub> O	3.18	2.54	2.87	2.63	3.05	2.87
K <sub>2</sub> O	1.93	5.57	2.88	3.47	2.70	3.71
P <sub>2</sub> O <sub>5</sub>	0.92	0.31	1.08	0.83	0.79	0.62
Total						
Trace elements (ppm)						
Ba	659	2502	1269	1269	1046	1562
Co	32	15	28	28	29	24
Cs	1	2	0	0	1	1
Ga	24	23	23	23	24	24
Hf	10	8	13	13	9	9
Nb	49	16	49	49	42	33
Rb	74	168	72	72	86	101
Sr	374	405	394	394	374	375
Ta	2	1	3	3	2	2
Th	4	11	4	4	6	8
U	0	1	0	0	0	1
V	168	87	175	175	151	128
Zr	392	345	550	550	382	369
Y	83	32	80	80	72	58
La	123	83	116	116	115	103
Ce	268	166	258	258	247	218
Pr	33	18	32	32	30	26
Nd	132	68	130	130	119	101
Sm	25	10	24	24	22	18
Eu	4	3	4	4	4	4
Gd	22	8	21	21	19	15
Tb	3	1	3	3	3	2
Dy	17	6	16	16	14	11
Ho	3	1	3	3	3	2
Er	9	3	8	8	8	6
Tm	1	0	1	1	1	1
Yb	7	3	7	7	6	5
Lu	1	0	1	1	1	1

\*  $C_{M1}$  calculated based on equation  $C_{M1} = X_A C_A + (1 - X_A) C_B$ , where the proportions of mafic component (X) is 0.79

\*\*  $C_{M2}$  calculated based on equation  $C_{M2} = X_A C_A + (1 - X_A) C_B$ , where the proportions of mafic component (X) is 0.51



In general, we conclude that the enclaves represent globules of mafic or hybrid magma that comingled with a more felsic host melt. The host felsic magma had a significant impact on the chemistry of the relatively small volume of the more mafic magma that intruded into the granitic magma chamber.

### Source of melts

The above interpretation raises the following questions, e.g., what was the source of the mafic magma? Was the magma source located in the mantle or crust? Is it the same source as for the felsic magma?

The A-type granitoids constitute an extremely diverse group of felsic rocks and their genesis is broadly discussed (cf. Bonin 2007; Dall'Agnol et al. 2012; Johansson 2023). Many authors associate the origin of A-type granites with crustal anatexis promoted by magmatic underplating (Rämö and Haapala 1995; Dall'Agnol et al. 1999, 2005). On the other hand, Eby (1990) and Bonin (2007) suggested that some A-type granitoids were derived directly from a mantle source.

The felsic rocks of the Krasnopol intrusion are ferroan (Fig. 4E) and oxidized A-type granitoids with metaluminous composition (Fig. 4B). According to Eby's classification (1992), they belong to anorogenic granites, related to average continental crust or arc-type sources (A2-type; Fig. 4H), which implies the differentiation of tholeiitic basalts or partial melting of the deepest part of the continental crust with varied composition as a source of magma. Nevertheless, the oxidized nature of the Krasnopol granitoids argues against a tholeiitic source (Frost and Frost 1997) and points towards a crustal origin (Clemens et al. 1986; Creaser et al. 1991; Dall'Agnol and de Oliveira 2007; Ballouard et al. 2020). Therefore, the partial melting of crustal rocks is the preferred genetic model for the A-type Krasnopol granitoids.

Ballouard et al. (2020) have suggested that the source of A<sub>2</sub>-type granitoids may be located in the deep parts of the crust consisting of amphibolite to lower granulite-facies rocks. Relatively low pressures calculated for the Krasnopol intrusion (4.3–4.5 kbar; Al-in-amphibole geobarometer; Mutch et al. 2016) indicate a shallow crystallization level. Nevertheless, the formation of the Proterozoic massif-type anorthosites is usually explained by polybaric crystallization, which starts at depths of 45–50 km (ca. 10–13 kbar) and continues at the final level of the emplacement at depths corresponding to 3–5 kbar (e.g., Ashwal 1993; Longhi et al. 1993, 1999; Wiszniewska et al. 2002). Recently a two-stage magmatic evolution for the Suwałki anorthosites and granitoids of the MC AMCG suite was documented (Wiszniewska and Krzemińska 2021). Therefore, it is likely that the early stage of the Krasnopol granitoid crystallization took place under similar pressure conditions (10–13 kbar) as in the case of anorthosites, i.e., in the lower crust. This agrees with the temperatures obtained from the clinopyroxene–liquid

thermometer (mean = 1005 °C), which suggests that pyroxene crystallized at high temperatures at considerable depths. Moreover, the granitoids display negative  $\epsilon\text{Nd}_{(1507)}$  values (from -3.8 to -4.0) and initial  $^{87}\text{Sr}/^{86}\text{Sr}$  ratios ranging from 0.7084 to 0.7138 (Table 2), which additionally confirms a dominant crustal role in their genesis. Thus, a mildly hydrous amphibolitic source of the lower crust is proposed for the Krasnopol granitoids.

Although the magma source of the granitoid rocks from the Krasnopol intrusion is certainly crustal, the source of mafic magma is more enigmatic. The different  $^{87}\text{Rb}/^{86}\text{Sr}$  isotope ratios of granitoids (0.86–0.99) and enclaves (0.56–0.70) indicate their different source composition. As it was stressed above, all of the enclaves have been largely modified by differentiation, assimilation at crustal depth, subsolidus processes and mixing with the granitoid melts. Hence, they do not strictly represent primary mafic magma composition.

Nevertheless, the slightly subchondritic  $\epsilon\text{Nd}_{(1507)}$  values (from -2.6 to -3.8) for the enclaves and lower, compared to the granitoids,  $^{87}\text{Sr}/^{86}\text{Sr}$  initial ratios (0.7052–0.7075), and a clear shift toward more mafic component in their source (Fig. 9) suggest a contribution of a mafic (mantle) material, and thus the formation of the mafic melts due to i) remelting of a juvenile mafic crust, ii) melting of the mantle source and subsequent crustal contamination during emplacement or iii) mantle-crustal source mixing. Moreover, the mantle origin of the enclaves is supported by the low  $\text{SiO}_2$  content in the most primitive (silica-poor) samples (Kr-6-37; 45.5 wt%  $\text{SiO}_2$ ), whereas the trace element

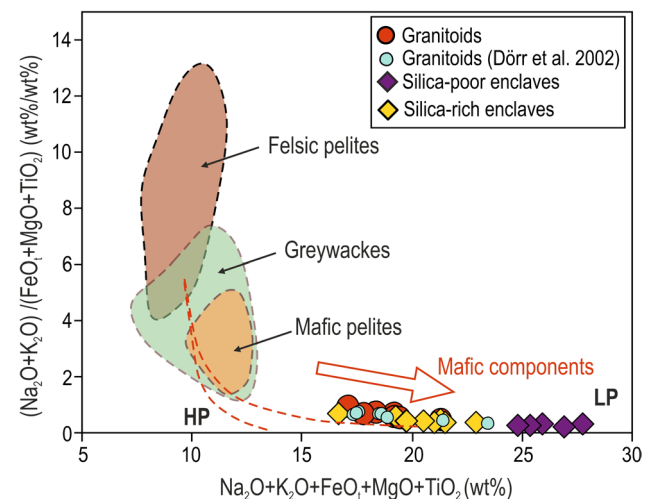


**Fig. 9** The  $(\text{Na}_2\text{O} + \text{K}_2\text{O}) / (\text{FeO}_1 + \text{MgO} + \text{TiO}_2)$  versus  $(\text{Na}_2\text{O} + \text{K}_2\text{O}) / (\text{FeO}_1 + \text{MgO} + \text{TiO}_2)$  diagram for the Krasnopol PIG-6 borehole granitoid rocks and enclaves discriminating between anatexitic melts from felsic pelite, graywacke and mafic pelite protoliths. Domains as in from Patiño Douce (1999). LP and HP show the composition of melts at low pressure ( $\leq 5$  kbar) and high pressure (12–15 kbar)

pattern (Fig. 6D), coupled with low Cr and Ni concentration (mostly below detection limits; Table 1) and low MgO content suggest a (lower) crustal origin. In the Th/Yb versus Nb/Yb diagram (Pearce 2008), part of the enclaves lie close to the field of enriched mantle-derived rocks (E-MORB) characteristics, confirming a greater involvement of incompatible elements than would be expected for a depleted mantle (Fig. 10). The  $T_{Nd}$  model ages of 2.05–2.11 Ga (Table 2) and the concurrent lack of the crust older than 1.8 Ga within the southwestern part of Fennoscandia support the conclusion that the re-melted Late Paleoproterozoic crustal component played a significant role. The location of the enclaves within the upper limits of the local Paleoproterozoic crust (Mazowsze Domain) field (Fig. 7; Krzemińska et al. 2017) indicates that the juvenile material contributed to the formation of the enclaves. Therefore, we believe that the magma parental to the enclaves most likely originated from a mixed source, i.e., sub-continental lithospheric mantle mixed with juvenile mafic crust.

The formation of such mixed mantle-crustal melts can be linked to the ‘crustal tongue melting’ model originally proposed by Duchesne et al. (1999), in which the crustal tongue of lower mafic crust is dragged into the upper mantle as a result of the former subduction of the older continental plate. Subsequent asthenospheric uprise and melting of the sub-continental lithospheric mantle with underthrust lower crust triggered crustal anatexis and teneration of more felsic magma (Fig. 11) at slightly higher depths. The reactivation

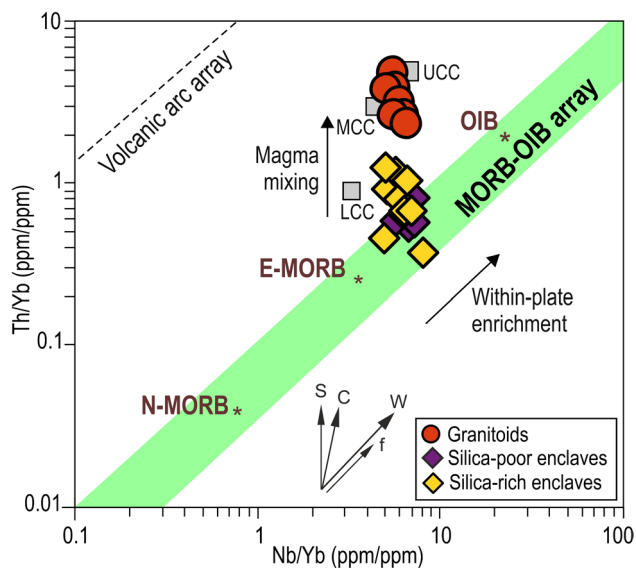


**Fig. 10** Th/Yb versus Nb/Yb diagram (after Pearce 2008) for the Krasnopolez borehole granitoid rocks and enclaves. The bold arrows in the bottom right are S=subduction component, C=crustal contaminant component, W=within plate, and f=fractional crystallisation vectors

of pre-existing lineaments caused the migration of magma (sensu Duchesne et al. 1999). As a consequence, the two coeval melts were derived from different depths and various types of protoliths.

Such a model has been already implemented for the origin of other granitic intrusions (Duchesne et al. 2010) and anorthosite massifs (Wiszniewska et al. 2002) of ca. 1.5 Ga AMCG magmatism of the Mazury Complex. Moreover, it is consistent with a hypothesis proposed by Vander Auwera et al. (2008), who suggested that hornblende-bearing granite was formed from a mildly hydrous amphibolitic mafic source, in contrast to anorthositic magma generated by the melting of a dry granulitic mafic source (Longhi et al. 1999). At this stage, melting of other domains of the lower crust could also have occurred resulting in the formation of the primary mafic melt of the studied enclaves. This melt is enriched in rare earth elements (REEs) and other trace elements and has a different isotopic composition than the granitoid host rocks (Fig. 11). It is possible that these water-enriched mafic magmas could significantly facilitate the dehydration melting of surrounding rocks, resulting in the formation of hydrous crustal melts (Annen et al. 2006).

Therefore, we suggest that the mafic melts, precursors of the enclaves, were formed by melting of the delaminated mafic lower crust that was dragged into the upper mantle (Fig. 11). The melting of the lower crust was accompanied

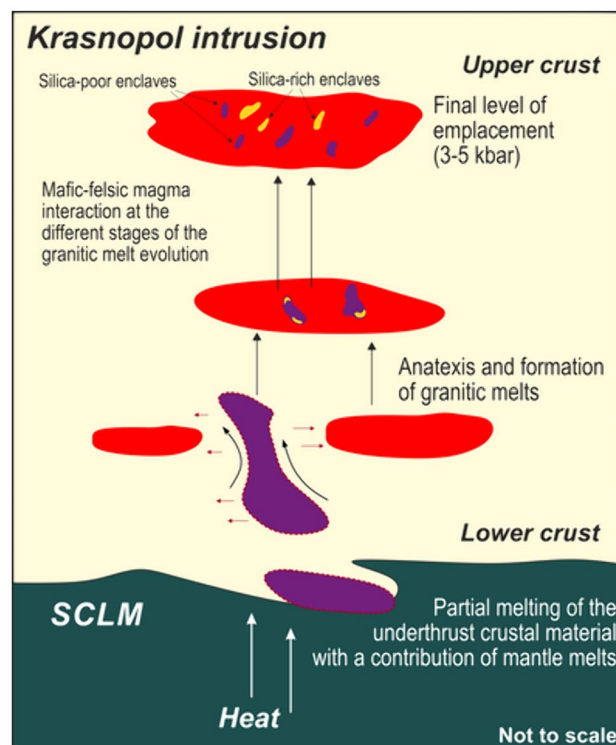


**Fig. 11** Model for the formation of the Krasnopolez intrusion. SCLM: subcontinental lithosphere mantle enclaves

by mixing with the subcontinental lithospheric mantle. The subsequent ascent of the hot mafic melts triggered anatexis of the overlying amphibolitic crust, resulting in the formation of the felsic melts (granitoid precursors). The two melts were mixed in different degrees, resulting in a variety of enclave compositions represented by globules of more mafic, hybrid magma that mingled with the more felsic host magma. The partly crystallized body was subsequently emplaced at the upper crustal level, forming the Krasnopol intrusion, which is evident by similar emplacement  $p$ – $T$  conditions, observed for the enclaves and host granitoids. This suggests that mafic-felsic melt interaction may have occurred at depths corresponding to approximately 4.3–4.5 kbar (the level of emplacement and equivalent to a shallow crustal level) or even during crystal mush ascent, as evidenced by the elongated morphology of the enclaves.

## Conclusions

The Krasnopol intrusion of the Mesoproterozoic Mazury Complex is a small magmatic body emplaced within the Paleoproterozoic crust of the East European Craton. Whole-rock geochemical studies, Sr–Nd isotope measurements and major and trace element geochemical modelling allow several conclusions to be drawn: (i) The Krasnopol intrusion is composed of porphyritic monzonite and granodiorite with numerous magmatic enclaves. The geochemical composition of the granitoids, i.e., metaluminous and ferroan character, elevated contents of REEs and LILEs, points to their A-type ( $A_2$ -subtype) affinity. (ii) The field and petrographic features of magmatic enclaves such as spherical and ellipsoidal shapes and diffuse/lobate contacts with host granitoids, as well as acicular apatites, and resorbed feldspar megacrysts with poikilitic textures, indicate the mixing of coexisting mafic and felsic magmas. (iii) Petrographic, geochemical and isotopic characteristics of the enclaves indicate that their parental magmas were derived from a hybrid source, mixture of sub-continental lithospheric mantle with juvenile mafic crust. (iv) The subsequent ascent of the hot, water-enriched mafic melts triggered anatexis of the overlying the Paleoproterozoic lower crust of amphibolitic composition, resulting in the formation of the granitic melts.

**Supplementary Information** The online version contains supplementary material available at <https://doi.org/10.1007/s00710-024-00866-1>.

**Acknowledgements** The whole-rock chemical analyses were conducted in the laboratories of the Bureau Veritas Commodities Ltd., Vancouver, Canada, while the chemical analyses of minerals were carried out in the Electron Microprobe Laboratory at the Inter-Institute Microanalytical Complex for Minerals and Synthetic Substances, Warsaw University, Poland. The Nd isotopic analyses were

performed in the Isotope Laboratory of the Adam Mickiewicz University in Poznań, Poland. We would like to express our gratitude to Beata Marciniak-Maliszewska for her assistance in the EPMA laboratory. We would also like to thank two anonymous reviewers for their helpful suggestions and comments relating to this manuscript. Furthermore, we would like to thank the editors Xisheng Xu and Lutz Nasdala for their insightful comments that helped improve the manuscript.

**Funding** This research was financially supported by a grant from the National Science Centre (NCN; grant number 2019/33/N/ST10/00944) to AGG.

**Open Access** This article is licensed under a Creative Commons Attribution 4.0 International License, which permits use, sharing, adaptation, distribution and reproduction in any medium or format, as long as you give appropriate credit to the original author(s) and the source, provide a link to the Creative Commons licence, and indicate if changes were made. The images or other third party material in this article are included in the article's Creative Commons licence, unless indicated otherwise in a credit line to the material. If material is not included in the article's Creative Commons licence and your intended use is not permitted by statutory regulation or exceeds the permitted use, you will need to obtain permission directly from the copyright holder. To view a copy of this licence, visit <http://creativecommons.org/licenses/by/4.0/>.

## References

- Anderson JL, Morrison J (2005) Ilmenite, magnetite, and peraluminous Mesoproterozoic anorogenic granites of Laurentia and Baltica. *Lithos* 80:45–60
- Anderson JL, Smith DR (1995) The effects of temperature and  $fO_2$  on the Al-in-hornblende barometer. *Am Mineral* 80:549–559
- Annen C, Blundy JD, Sparks RJS (2006) The genesis of intermediate and silicic magmas in deep crustal hot zones. *J Petrol* 47:505–539
- Ashwal LD (1993) Proterozoic massif-type anorthosites. *Anorthosites, Minerals and Rocks*. Springer, Heidelberg, pp 82–218
- Bagiński B, Duchesne JC, Martin H, Wiszniewska J (2007) Isotopic and geochemical constraints on the evolution of the Mazury granitoids, NE Poland. In: Kozłowski A, Wiszniewska J (eds) *Granitoids in Poland*, AM Monograph No. 1. University of Warsaw, Warszawa, pp 11–30
- Bagiński B, Duchesne JC, Vander Auwera J, Martin H, Wiszniewska J (2001) Petrology and geochemistry of rapakivi-type granites from the crystalline basement of NE Poland. *Geol Q* 45:33–52
- Ballouard C, Massuyeau M, Elburg MA, Tappe S, Viljoen F, Brandenburg JT (2020) The magmatic and magmatic-hydrothermal evolution of felsic igneous rocks as seen through Nb-Ta geochemical fractionation, with implications for the origins of rare-metal mineralizations. *Earth Sci Rev* 203:1–31
- Barbarin B (2005) Mafic magmatic enclaves and mafic rocks associated with some granitoids of the central Sierra Nevada batholith, California: nature, origin, and relations with the hosts. *Lithos* 80:155–177
- Barbarin B, Didier J (1991) Review of the main hypothesis proposed for the genesis and evolution of mafic microgranular enclaves. In: Didier J, Barbarin B (eds) *Enclaves and Granite Petrology*, Developments in Petrology 13. Elsevier, Amsterdam, pp 367–373
- Blundy J, Wood B (2003a) Mineral-melt partitioning of uranium, thorium and their daughters. *Rev Mineral Geochem* 52:59–123

- Blundy J, Wood B (2003b) Partitioning of trace elements between crystals and melts. *Earth Planet Sci Lett* 210:383–397
- Bogaerts M, Scaillet B, Vander Auwera J (2006) Phase equilibria of the Lyngdal granodiorite (Norway): implications for the origin of metaluminous ferroan granitoids. *J Petrol* 47:2405–2431
- Bogdanova SV, Gorbatshev R, Skridlaite G, Soesoo A, Taran L, Kurlovich D (2015) Trans-Baltic Palaeoproterozoic correlations towards the reconstruction of supercontinent Columbia/Nuna. *Precambrian Res* 259:5–33
- Bonin B (2007) A-type granites and related rocks: evolution of a concept, problems and prospects. *Lithos* 97:29
- Castro A, Moreno-Ventas I, de La Rosa JD (1990) Microgranular enclaves as indicators of hybridization processes in granitoid rocks, Hercynian Belt, Spain. *Geol J* 25:391–404
- Chappell BW, White AJR (1991) Restite enclaves and the restite model. In: Didier J, Barbarin B (eds) *Enclaves and granite petrology, developments in petrology 13*. Elsevier, Amsterdam, pp 375–381
- Chappell BW, White AJR, Wyborn D (1987) The importance of residual source material (restite) in granite petrogenesis. *J Petrol* 28:1111–1138
- Chen S, Niu Y, Sun W, Zhang Y, Li J, Guo P, Sun P (2015) On the origin of mafic magmatic enclaves (MMEs) in syncollisional granitoids: evidence from the Baojishan pluton in the North Qilian Orogen, China. *Mineral Petrol* 109:577–596
- Clemens JD, Holloway JR, White AJR (1986) Origin of an A-type granite; experimental constraints. *Am Mineral* 71:317–324
- Collins WJ, Richards SR, Healy BE, Ellison PI (2000) Origin of heterogeneous mafic enclaves by two-stage hybridization in magma conduits (dykes) below and in granitic magma chambers. *Earth Environ Sci Trans R Soc Edinb* 91:27–45
- Creaser RA, Price RC, Wormald RJ (1991) A-type granites revisited: assessment of a residual-source model. *Geology* 19:163–166
- Crisp LJ, Berry AJ (2022) A new model for zircon saturation in silicate melts. *Contrib Mineral Petr* 177(71):1–24
- Čečys A, Benn K (2007) Emplacement and deformation of the ca. 1.45 Ga Karlshamn granitoid pluton, southeastern Sweden, during ENE-WSW Danopolonian shortening. *Int J Earth Sci* 96:397–414
- Čečys A, Bogdanova S, Jansson C, Bibikova E, Kornfält K-A (2002) The Stenshuvudand Tåghusa granitoids: new representatives of mesoproterozoic magmatism in southern Sweden. *GFF* 124:149–162
- Dadlez R, Grad M, Guterch A (2005) Crustal structure below the Polish Basin: is it composed of proximal terranes derived from Baltica? *Tectonophysics* 411:111–128
- Dall'Agnol R, de Oliveira DC (2007) Oxidized, magnetite-series, rapakivi-type granites of Carajás, Brazil: implications for classification and petrogenesis of A-type granites. *Lithos* 93:215–233
- Dall'Agnol R, Frost CD, Rämö OT (2012) IGCP project 510 A-type granites and related rocks through time: project vita, results, and contribution to granite research. *Lithos* 151:1–16
- Dall'Agnol R, Scaillet B, Pichavant M (1999) An experimental study of a lower Proterozoic A-type granite from the Eastern Amazonian Craton, Brazil. *J Petrol* 40:1673–1698
- Dall'Agnol R, Teixeira NP, Rämö OT, Moura CA, Macambira MJ, de Oliveira DC (2005) Petrogenesis of the Paleoproterozoic rapakivi A-type granites of the Archean Carajás metallogenic province, Brazil. *Lithos* 80:101–129
- DePaolo DJ (1981) Trace element and isotopic effect of combined wall-rock assimilation and fractional crystallization. *Earth Planet Sci Lett* 53:189–202
- DePaolo DJ (1983) Geochemical evolution of the crust and mantle. *Rev Geophys* 21:1347–1358
- Didier J (1984) The problem of enclaves in granitic rocks: a review of recent ideas on their origin. In: Xu KQ, Tu GC (eds) *Proceedings of international symposium on geology of granites and their metallogenic relations*. Nanjing University Science Press, Nanjing and Beijing, China, pp 137–144
- Didier J, Barbarin B (eds) (1991) *Enclaves and granite petrology, developments in petrology 13*. Elsevier, Amsterdam, p 625
- Didier JD (ed) (1973) *Granites and their enclaves*. In: *developments in petrology 3*. Elsevier, Amsterdam, p 393
- Domańska-Siuda J, Bagiński NK, Macdonald B, Kotowski J, Stachowicz M (2022) Chevkinite-group minerals in selected intrusions of the Mazury complex, North-Eastern Poland: insights into the formation of a titanite-like phase by hydrothermal alteration. *Mineral Petrol* 116:105–119
- Domańska-Siuda J, Słaby E, Szuszkiewicz A (2019) Ambiguous isotopic and geochemical signatures resulting from limited melt interactions in a seemingly composite pluton: a case study from the Strzegom-Sobótka Massif (Sudetes, Poland). *Int J Earth Sci* 108:031–962
- Donaire T, Pascual E, Pin C, Duthou JL (2005) Microgranular enclaves as evidence of rapid cooling in granitoid rocks: the case of the Los Pedroches granodiorite, Iberian Massif, Spain. *Contrib Mineral Petrol* 149:247–265
- Dopieralska J (2003) Neodymium isotopic composition of conodonts as a palaeoceanographic proxy in the Variscan oceanic system, Ph.D. thesis, Justus-Liebig-University, Giessen, 111 pp (available at <http://geb.uni-giessen.de/geb/volltexte/2003/1168/>)
- Dorais MJ, Lira R, Chen Y, Tingey D (1997) Origin of biotite-apatite-rich enclaves, Achala batholith, Argentina. *Contrib Mineral Petrol* 130:31–46
- Dörr W, Belka Z, Marheine D, Schastok J, Valverde-Vaquero P, Wiszniewska J (2002) U-Pb and Ar-Ar geochronology of anorogenic granite magmatism of the Mazury complex, NE Poland. *Precambrian Res* 119:101–120
- Duchesne JC, Liégeois JP, Vander Auwera J, Longhi J (1999) The crustal tongue melting model and the origin of massive anorthosites. *Terra Nova* 11:100–105
- Duchesne JC, Martin H, Bagiński B, Wiszniewska J, Vander Auwera J (2010) The origin of ferroan-potassic A-type granitoids: the case of the hornblende-biotite granite suite of the Mesoproterozoic Mazury complex, northeastern Poland. *Can Mineral* 48:947–968
- Eby GN (1990) The A-type granitoids: a review of their occurrence and chemical characteristics and speculations on their petrogenesis. *Lithos* 26:115–134
- Eby GN (1992) Chemical subdivision of the A-type granitoids: petrogenetic and tectonic implications. *Geology* 20:641–644
- Eklund O, Fröjdö S, Lindberg B (1994) Magma mixing, the petrogenetic link between anorthositic suites and rapakivi granites, Åland, SW Finland. *Mineral Petrol* 50:3–19
- Elburg MA (1996) Evidence of isotopic equilibration between microgranitoid enclaves and host granodiorite, Warburton Granodiorite, Lachlan Fold Belt, Australia. *Lithos* 38:1–22
- Fershtater GB, Borodina NS (1977) Petrology of autoliths in granitic rocks. *Int Geol Rev* 19:458–468
- Fershtater GB, Borodina NS (1991) Enclaves in the hercynian granitoids of the Ural Mountains, USSR. In: Didier J, Barbarin B (eds) *Enclaves and granite petrology, developments in petrology 13*. Elsevier, Amsterdam, pp 83–94
- Fleet ME, Barnett RL (1978) Al<sup>IV</sup>/Al<sup>VI</sup> partitioning in calciferous amphiboles from the frood mine, Sudbury, Ontario. *Can Mineral* 16:527–532
- Flood RH, Shaw SE (2014) Microgranitoid enclaves in the felsic Loonga monzogranite, New England Batholith, Australia: pressure quench cumulates. *Lithos* 198:92–102
- Fourcade S, Allegre CJ (1981) Trace elements behavior in granite genesis: a case study the calc-alkaline plutonic association from the Querigut complex (Pyrenées, France). *Contrib Mineral Petrol* 76:177–195



- Frost BR, Barnes CG, Collins WJ, Arculus RJ, Ellis DJ, Frost CD (2001) A geochemical classification for granitic rocks. *J Petrol* 42:2033–2048
- Frost CD, Frost BR (1997) Reduced rapakivi-type granites: the tholeiite connection. *Geology* 25:647–650
- Grabarczyk A, Wiszniewska J (2019) Comparative geochemical assessment of jotunite rocks from the Suwałki Massif and the Sejny Intrusion (NE Poland). *Acta Geol Pol* 69:513–529
- Gorbatshev R, Bogdanova S (1993) Frontiers in the Baltic shield. *Precambr Res* 64:3–21
- Guimarães IP, da Silva Filho AF, Melo SC, Macambira MB (2005) Petrogenesis of A-type granitoids from the Alto Moxoto and Alto Pajeu Terranes of the Borborema Province, NE Brazil: constraints from geochemistry and isotopic composition. *Gondwana Res* 8:347–362
- Haapala I, Rämö OT (1999) Rapakivi granites and related rocks: an introduction. *Precambrian Res* 95:1–7
- Henry D, Guidotti C, Thomson J (2005) The Ti-saturation surface for low-to-medium pressure metapelitic biotites: implications for geothermometry and Ti-substitution mechanism. *Am Mineral* 90:316–328
- Hibbard MJ (1991) Textural anatomy of twelve magma-mixed granitoid systems. In: Didier J, Barbarin B (eds) *Enclaves and granite petrology, developments in petrology 13*. Elsevier, Amsterdam, pp 431–444
- Irvine TN, Baragar WRA (1971) A guide to the chemical classification of the common volcanic rocks. *Can J Earth Sci* 8:523–548
- Jacobsen SB, Wasserburg GJ (1980) Sm-Nd isotopic evolution of chondrites. *Earth Planet Sci Lett* 50:139–155
- Johansson Å (2023) A tentative model for the origin of A-type granitoids. *Minerals* 13:236
- Johansson Å, Waight T, Andersen T, Simonsen SL (2016) Geochemistry and petrogenesis of Mesoproterozoic A-type granitoids from the Danish island of Bornholm, Southern Fennoscandia. *Lithos* 244:94–108
- Johnston AD, Wyllie PJ (1988) Interaction of granitic and basic magmas: experimental observations on contamination processes at 10 kbar with H<sub>2</sub>O. *Contrib Mineral Petrol* 98:352–362
- Kontonikas-Charos A, Ehrig K, Cook NJ, Ciobanu CL (2023) Mafic mineral clots and microgranular enclaves in A-type Hiltaba Suite granites from the Gawler Craton, South Australia: origins and implications. *Lithos* 446–447:107114
- Krzemińska E, Krzemiński L, Petecki Z, Wiszniewska J, Salwa S, Zaba J, Gaidzik K, Williams IS, Rosowiecka O, Taran L, Johansson Å, Pécský Z, Demaiffe D, Grabowski J, Zieliński G (2017) Geological map of crystalline basement in the Polish part of the East European platform 1:1 000 000. Polish Geological Institute, Warsaw, p 58
- Kumar S (2020) Schedule of mafic to hybrid magma injections into crystallizing felsic magma chambers and resultant geometry of enclaves in granites: new field and petrographic observations from Ladakh Batholith, Trans-Himalaya. *India Front Earth Sci* 8:551097
- Kumar S, Rino V (2006) Mineralogy and geochemistry of microgranular enclaves in Palaeoproterozoic Malanjhand granitoids, central India: evidence of magma mixing, mingling, and chemical equilibration. *Contrib Mineral Petrol* 152:591–609
- Kumar S, Rino V, Pal AB (2004) Field evidence of magma mixing from microgranular enclaves hosted in Palaeoproterozoic Malanjhand granitoids, central India. *Gondwana Res* 7:539–548
- Leake BE (1971) On aluminous and edenitic hornblendes. *Mineral Mag* 38:389–405
- Longhi J, Fram MS, Vander Auwera J, Montieth JN (1993) Pressure effects, kinetics, and rheology of anorthositic and related magmas. *Am Mineral* 78:1016–1030
- Longhi J, Vander Auwera J, Fram MS, Duchesne JC (1999) Some phase equilibrium constraints on the origin of proterozoic (massif) anorthosites and related rocks. *J Petrol* 40:339–362
- Merlet C (1994) An accurate computer correction program for quantitative electron probe microanalysis. *Mikrochim Acta* 114:363–376
- Mutch EJJ, Blundy JD, Tattitch BC, Cooper FJ, Brooker RA (2016) An experimental study of amphibole stability in low-pressure granitic magmas and a revised Al-in-hornblende geobarometer. *Contrib Mineral Petrol* 171:85
- Nakamura N (1974) Determination of REE, Ba, Fe, Mg, Na and K in carbonaceous and ordinary chondrites. *Geochim Cosmochim Acta* 38:757–775
- Narshimha C, Kumar S (2023) Peraluminous A-type granites formed through synchronous fractionation, magma mixing, mingling, and undercooling: evidence from microgranular enclaves and host mesoproterozoic Kanigiri granite pluton, Nellore Schist Belt, Southeast India. *Acta Geochim* 42:603–636
- Naney MT, Swanson SE (1980) The effect of Fe and Mg on crystallization in granitic systems. *Am Mineral* 65:639–653
- Nejbert K, Bagiński B, Kotowski J, Jokubauskas P, Jurewicz E, Macdonald R (2020) Chevkinite-group minerals in Poland. *Acta Geol Pol* 70:97–106
- Otten MT (1984) The origin of brown hornblende in the Artfjället gabbro and dolerites. *Contrib Mineral Petrol* 86:189–199
- Patiño Douce AE (1999) What do experiments tell us about the relative contributions of crust and mantle to the origin of granitic magmas? *Geol Soc Spec Publ London* 168(1):55–75
- Pearce JA (2008) Geochemical fingerprinting of oceanic basalts with applications to ophiolite classification and the search for Archean oceanic crust. *Lithos* 100:14–48
- Perugini D, De Campos CP, Dingwell DB, Petrelli M, Poli G (2008) Trace element mobility during magma mixing: preliminary experimental results. *Chem Geol* 256:146–157
- Perugini D, Petrelli M, Poli G (2006) Diffusive fractionation of trace elements by chaotic mixing of magmas. *Earth Planet Sci Lett* 243:669–680
- Perugini D, Poli G (2012) The mixing of magmas in plutonic and volcanic environments: analogies and differences. *Lithos* 153:261–277
- Perugini D, Poli G, Mazzuoli R (2003) Chaotic advection, fractals and diffusion during mixing of magmas: evidence from lava flows. *J Volcanol Geotherm* 124:255–279
- Petecki Z, Wiszniewska J (2021) Internal structure of the buried Suwałki Anorthosite Massif (East European Craton, NE Poland) based on borehole, magnetic and gravity data combined with new petrological results. *Geol Q* 65:4
- Pin C, Briot D, Bassin C, Poitrasson F (1994) Concomitant separation of strontium and samarium-neodymium for isotopic analysis in silicate samples, based on specific extraction chromatography. *Anal Chim Acta* 298:209–222
- Putirka K (2008) Thermometers and barometers for volcanic systems. In: Putirka K, Tepley F (eds) *Minerals, inclusions and volcanic processes*. *Rev Mineral Geochem, Mineralogical Soc Am*, vol 69. pp 61–120
- Rämö OT, Haapala I (1995) One hundred years of rapakivi granite. *Mineral Petrol* 52:129–185
- Rämö OT, Huhma H, Kirs J (1996) Radiogenic isotopes of the Estonian and Latvian rapakivi granite suites: new data from the concealed Precambrian of the East European Craton. *Precambrian Res* 79:209–226
- Reid JB, Murray DP, Hermes OD, Steig EJ (1993) Fractional crystallization in granites of the Sierra Nevada: how important is it? *Geology* 21:587–590

- Rickwood PC (1989) Boundary lines within petrologic diagrams which use oxides of major and minor elements. *Lithos* 22(4):247–263
- Ridolfi F, Renzulli A, Puerini M (2010) Stability and chemical equilibrium of amphibole in calc-alkaline magmas: an overview, new thermobarometric formulations and application to subduction-related volcanoes. *Contrib Mineral Petrol* 160:45–66
- Salminen J, Elming SÅ, Mertanen S, Wang C, Almqvist B, Moakhar MO (2021) Paleomagnetic studies of rapakivi complexes in the Fennoscandian shield—Implications to the origin of Proterozoic massif-type anorthosite magmatism. *Precambrian Res* 365:106406
- Salonsaari PT, Haapala I (1994) The Jaala-Iitti Rapakivi complex. An example of bimodal magmatism and hybridization in the Wiborg rapakivi batholith, Southeastern Finland. *Mineral Petrol* 50:21–34
- Shand SJ (1943) Eruptive rocks; their genesis, composition, classification, and their relation to ore-deposits, with a chapter on meteorites. John Wiley & Sons, New York, 488 pp
- Shellnutt JG, Jahn B-M, Dostal J (2010) Elemental and Sr–Nd isotope geochemistry of microgranular enclaves from peralkaline A-type granitic plutons of the Emeishan large igneous province, SW China. *Lithos* 119:34–46
- Shumlyanskyy L, Hawkesworth C, Billström K, Bogdanova S, Mytrokhyn O, Romer R, Dhuime B, Claesson S, Ernst R, Whitehouse M, Bilan O (2017) The origin of the Palaeoproterozoic AMCG complexes in the Ukrainian shield: new U–Pb ages and Hf isotopes in zircon. *Precambrian Res* 292:216–239
- Skridlaite G, Bagiński B, Whitehouse M (2008) Significance of ~1.5 Ga zircon and monazite ages from charnockites in southern Lithuania and NE Poland. *Gondwana Res* 14:663–674
- Skridlaite G, Siliuskas L, Whitehouse MJ, Johansson Å, Rimsa A (2021) On the origin and evolution of the 1.86–1.76 Ga Mid-Baltic Belt in the western East European Craton. *Precambrian Res* 367:106403
- Skridlaite G, Wiszniewska J, Duchesne JC (2003) Ferro-potassic A-type granites and related rocks in NE Poland and S Lithuania: west of the East European Craton. *Precambrian Res* 124:305–326
- Słaby E, Martin H (2008) Mafic and felsic magma interaction in granites: the Hercynian Karkonosze Pluton (Sudetes, Bohemian Massif). *J Petrol* 49:353–391
- Sun SS, McDonough WS (1989) Chemical and isotopic systematics of oceanic basalts: implications for mantle composition and processes. *Geol Soc Spec Publ* 42:313–345
- Teng FZ, Rudnick RL, McDonough WF, Wu FY (2009) Lithium isotopic systematics of A-type granites and their mafic enclaves: further constraints on the Li isotopic composition of the continental crust. *Chem Geol* 262:370–379
- Vander Auwera J, Bogaerts M, Bolle O, Longhi J (2008) Genesis of intermediate igneous rocks at the end of the Sveconorwegian (Grenvillian) orogeny (S Norway) and their contribution to intracrustal differentiation. *Contrib Mineral Petrol* 156:721–743
- Vejelyte I, Bogdanova SV, Skridlaite G (2015) Early Mesoproterozoic magmatism in northwestern Lithuania: a new U–Pb zircon dating. *Estonian J Earth Sci* 64:189–198.
- Vernon RH (1983) Restite, xenoliths and microgranitoid enclaves in granites. *J Proc - R Soc N S W* 116:77–109
- Vernon RH (1984) Microgranitoid enclaves in granites-globules of hybrid magma quenched in a plutonic environment. *Nature* 309:438–439
- Vernon RH (1990) Crystallization and hybridism in microgranitoid enclave magmas: microstructural evidence. *J Geophys Res Solid Earth* 95:17849–17859
- Vernon RH (1991) Interpretation of microstructures of micro-granitoid enclaves. In: Didier J, Barbarin B (eds) *Enclaves and granite petrology, developments in petrology 13*. Elsevier, Amsterdam, pp 277–291
- Vernon RH, Etheridge MA, Wall VJ (1988) Shape and microstructure of the microgranitoid enclaves: indicators of magma mingling and flow. *Lithos* 22:1–11
- Waight TE, Frei D, Storey M (2012) Geochronological constraints on granitic magmatism, deformation, cooling and uplift on Bornholm, Denmark. *Bull Geol Soc Den* 60:23–46
- Wang XX, Wang T, Castro A, Pedreira R, Lu XX, Xiao QH (2011) Triassic granitoids of the Qinling orogen, central China: genetic relationship of enclaves and rapakivi-textured rocks. *Lithos* 126:369–387
- Whalen JB, Currie KL, Chappell BW (1987) A-type granites: Geochemical characteristics, discrimination, and petrogenesis. *Contrib Mineral Petrol* 95:407–419
- White AJR, Chappell BW (1977) Ultrametamorphism and granitoid genesis. *Tectonophysics* 43:7–22
- Wiebe RA (1994) Silicic magma chambers as traps for basaltic magmas: the Cadillac Mountain intrusive complex, Mount Desert island, Maine. *J Geol* 102:423–427
- Wiszniewska J, Claesson S, Stein H, Vander Auwera J, Duchesne JC (2002) The north eastern Polish anorthosite massifs: petrological, geochemical and isotopic evidence for a crustal derivation. *Terra Nova* 14:451–460
- Wiszniewska J, Krzemińska E (2021) Advances in geochronology in the Suwałki anorthosite massif and subsequent granite veins, northeastern Poland. *Precambrian Res* 361:106265
- Wiszniewska J, Kusiak MA, Krzemińska E, Dörr W, Suzuki K (2007) Mesoproterozoic AMCG granitoids in the Mazury complex, NE Poland—a geochronological update. In: Kozłowski A, Wiszniewska J (eds) *Granitoids in Poland*, AM Monograph No. 1. University of Warsaw, Warszawa, pp 31–39
- Yang JH, Wu FY, Chung SL, Wilde SA, Chu MF (2006) A hybrid origin for the Qianshan A-type granite, northeast China: geochemical and Sr–Nd–Hf isotopic evidence. *Lithos* 89:89–106
- Zariņš K, Johansson Å (2009) U–Pb geochronology of gneisses and granitoids from the Danish island of Bornholm: new evidence for 1.47–1.45 Ga magmatism at the southwestern margin of the East European Craton. *Int J Earth Sci* 98:1561–1580

**Publisher's Note** Springer Nature remains neutral with regard to jurisdictional claims in published maps and institutional affiliations.